Himalayan Metamorphism and Its Tectonic Implications

Matthew J. Kohn

Department of Geosciences, Boise State University, Boise, Idaho 83725;
email: mattkohn@boisestate.edu

Keywords

Abstract

The Himalayan range exposes a spectacular assemblage of metamorphic rocks from the mid- and deep crust that have fostered numerous models of how the crust responds to continental collisions. Recent petrogenetically based petrologic and geochronologic studies elucidate processes with unprecedented resolution and critically test models that range from continuum processes to one-time events. The pronounced metamorphic inversion across the Main Central Thrust reflects continuum thrusting between ca. 15 and 20 Ma, whereas exposure of ultrahigh-pressure rocks in northwestern massifs and syntaxis granulites reflects singular early ($\geq$45 Ma) and late ($\leq$10 Ma) exhumation events. Multiple mechanisms including wedge collapse and flow of melt-weakened midcrust are debated to explain pressure-temperature trajectories, patterns of thinning, and thermal overprinting. A geochronologic revolution is under way in which spatially resolved compositions and ages of accessory minerals are combined in a petrogenetically valid context to recover specific temperature-time points and paths. Combined chemical and chronologic analysis of monazite is now well established and titanite is particularly promising, but recent zircon data raise questions about anatectic rocks and their use for investigating tectonism.

INTRODUCTION

Himalayan geology unquestionably has played a central role in shaping our understanding of orogenesis. After all, Himalayan thrust-belt architecture, rock-type distributions, geomorphology, and orogen-parallel and -perpendicular extension have given rise to numerous models—orogenic wedges, lower crustal flow, synorogenic magmatism, eclogite exhumation, origins of gneiss domes and oroclinal bends, etc.—and stimulated research linking geomorphic and tectonic processes. Metamorphic rocks have inspired and continue to inspire many of these models and thus warrant particular consideration. Compared with other orogens, two practical advantages attend Himalayan metamorphic studies. First, along-strike consistency of rock types and structures allows age-equivalent comparisons of different parts of the orogen and helps screen for local anomalies. Second, extreme youth facilitates chronologic analysis. For example, typical microanalytical uncertainties of 2% provide ≤1 Myr resolution in the Himalaya, whereas the same chronologic resolution in Paleozoic or Proterozoic orogens requires other analytical methods that attain <0.1 to 0.5% uncertainties.

This review is basically separated into two parts. The first and longer part documents patterns and summarizes regional geology, quantitative pressure-temperature conditions and paths, unusual occurrences of eclogites and granulites, and accessory mineral geochronology and geochemistry. The second part addresses tectonic models, emphasizing how observations distinguish (or not) among potential tectonic drivers. Given that over 600 articles on Himalayan metamorphism have been published, only a minority of studies can be discussed here. Metamorphic domes in southern Tibet and textural links between metamorphism and deformation are not considered. I also emphasize studies whose observations are reliably and quantitatively linked to petrogenesis and pressure-temperature-time evolution.

GEOLOGIC BACKGROUND: METAMORPHIC SANDWICHES AND ANOMALIES

Regional geology is described at length by Yin & Harrison (2000) and Yin (2006), so the following section focuses on only the most salient points related to metamorphism and its tectonic drivers. The Himalaya span approximately 2,000 km, from Pakistan in the west through northwestern India, Nepal, and Bhutan, to southeastern Tibet and northeastern India (**Figure 1**). Collision between India and Asia commenced ca. 50–55 Ma (e.g., see summary in Najman et al. 2010), but motion on major thrusts within the metamorphosed portion of the orogenic wedge generally commenced ca. 25 Ma. Overall, the orogen exhibits a distinct arcuate form, with sharp bends at the western (Nanga Parbat) and eastern (Namche Barwa) syntaxes (**Figure 1**), where major drainages cross the orogen.

A tripartite lithotectonic subdivision—Lesser, Greater, and Tethyan Himalayan Sequences (LHS, GHS, and THS, respectively)—frames Himalayan metamorphic studies (**Figure 1**). The LHS was emplaced above unmetamorphosed foreland sediments (Siwalik Group) along the Main Boundary Thrust (MBT). Numerous smaller thrusts have been proposed within the LHS, especially to form the Lesser Himalayan Duplex (LHD). This duplex is important structurally because it accommodated a significant portion of Indo-Asian convergence and tilted overlying LHS, GHS, and THS rock units to expose obliquely the Himalayan metamorphic core (DeCelles et al. 2001, Robinson et al. 2003). The GHS was emplaced above the LHS along the Main Central Thrust (MCT). Additional thrusts have been proposed within the GHS, but structural repetitions are less clear within this unit. All major thrusts are interpreted to have soled into a master detachment surface—the Main Himalayan Thrust (MHT). The THS shares broad stratigraphic similarities with the GHS, but in most regions was juxtaposed against it along a

---

Lesser Himalayan Sequence (LHS): mainly Proterozoic metasedimentary sequence, typically greenschist to amphibolite facies; occurs below the GHS

Greater Himalayan Sequence (GHS): Late Proterozoic to Paleozoic metasedimentary sequence, typically upper amphibolite to lower granulite facies; occurs above the LHS and below the THS

Tethyan Himalayan Sequence (THS): mainly Late Proterozoic to Mesozoic metasedimentary sequence, typically unmetamorphosed to lower amphibolite facies; occurs above the GHS

Main Boundary Thrust (MBT): thrust contact separating the LHS from foreland sediments (Siwaliks)

Lesser Himalayan Duplex (LHD): series of in-sequence thrusts in the LHS forming a duplex that arches overlying GHS and THS rocks

Main Central Thrust (MCT): thrust contact separating the GHS from the LHS
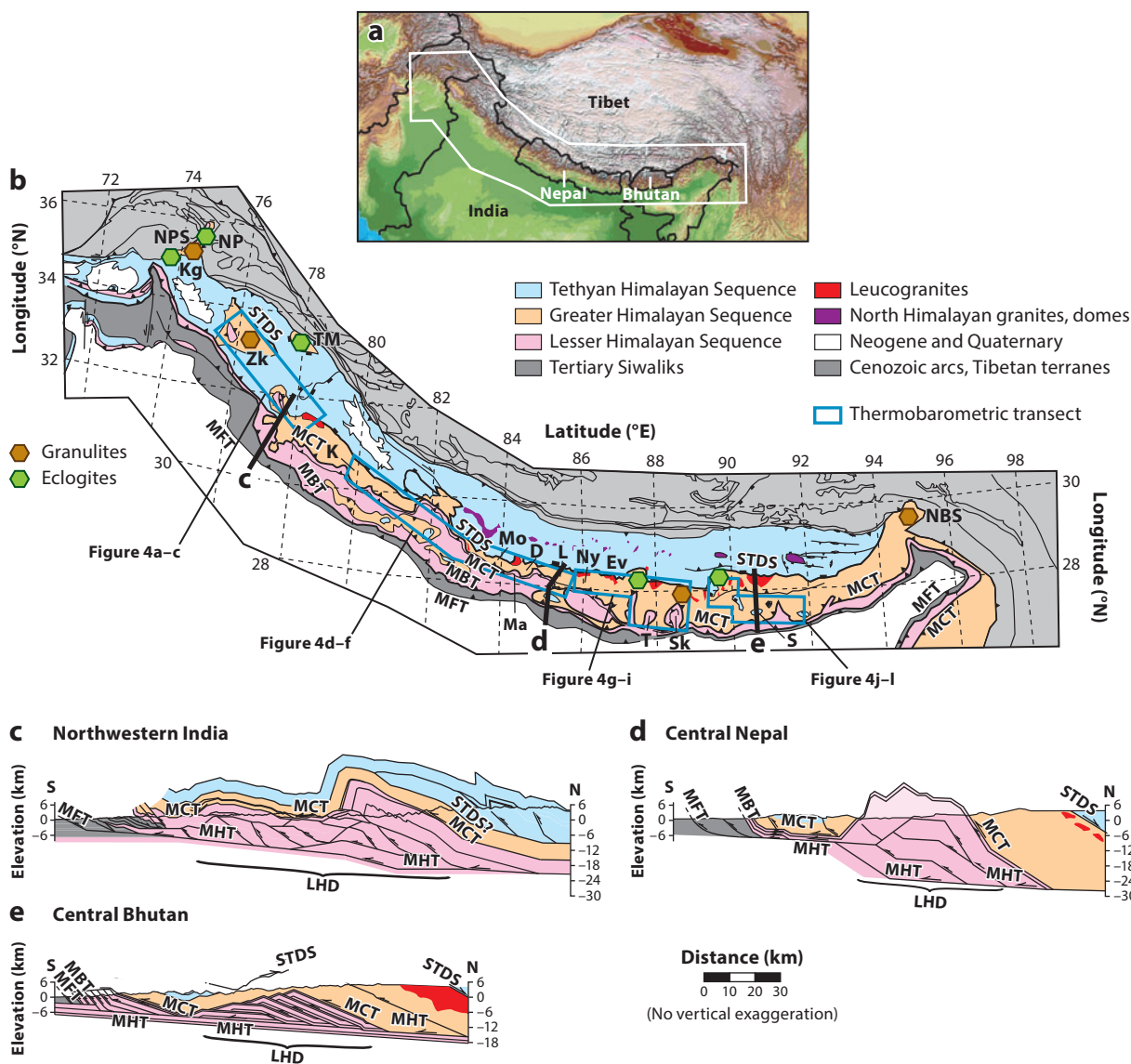
Figure 1

(*a*) Digital elevation model of the Himalaya and neighboring regions (Kohn 2007; modified with permission from the Mineralogical Society of America). The white polygon outlines the region illustrated in panel *b*. (*b*) Simplified regional geologic map of the Himalaya (modified from Yin & Harrison 2000) illustrating main lithotectonic units, general structural trends, locations of cross sections (*thick black lines*), thermobarometric transects (*blue boxes*), and eclogites and granulites (*hexagons*). (*c–e*) Western, central, and eastern cross sections (modified from Pearson & DeCelles 2005, Long et al. 2011, Webb et al. 2011). Pluton thicknesses are schematic. Geologic abbreviations: LHD, Lesser Himalayan Duplex; MBT, Main Boundary Thrust; MCT, Main Central Thrust; MFT, Main Frontal Thrust; MHT, Main Himalayan Thrust; STDS, South Tibetan Detachment System. Geographic abbreviations: D, Darondi; Ev, Everest; K, Kumaun; Kg, Kaghan; L, Langtang; Ma, Marsyandi; Mo, Modi; NP, Nanga Parbat; Ny, Nyalam; NBS, Namche Barwa syntaxis; NPS, Nanga Parbat syntaxis; Sk, Sikkim; TM, Tso Morari; Zk, Zanskar.

series of extensional shear structures called the South Tibetan Detachment System (STDS). The STDS could either merge with the MHT at depth (Burchfiel & Royden 1985) or shallow to the north, forming backthrusts (Yin 2006).

Composite geologic maps and cross sections (**Figure 1**) illustrate the consistency of stratigraphy and structure along strike. Although each area differs in detail, the LHS, GHS, THS, MBT, MCT, and STDS (with one possible exception) can nonetheless be traced for ∼2,000 km. Cross sections from the northwestern, central, and eastern Himalaya (**Figure 1**) consistently show a broad central duplex of LHS rocks that warps the MCT, LHS, GHS, and THS into a broad anticline. Toward the foreland, broad synclines and outliers of the THS and GHS are particularly obvious in Bhutan and central Nepal (**Figure 1**). Difficulties distinguishing GHS and THS lithologies in these outliers can cause divergent stratigraphic assignments. Toward the hinterland, the same LHS-GHS-THS units and the MCT and STDS dip uniformly to the north and northeast. Thus, the moderate northward dip on the MCT is not a primary feature; instead, the thrust formed with a shallow dip, similar to the modern MHT, and was passively tilted during later duplex formation (DeCelles et al. 2001, Robinson et al. 2003).

With respect to metamorphic distributions, the LHS-GHS-THS assemblage can be considered a metamorphic "sandwich," in which low-grade THS and LHS rocks bound intervening high-grade GHS rocks (**Figures 2** and **3**). The sandwich is generally higher grade in hinterland sections and lower grade in structural outliers closer to the foreland. In hinterland sections that have been studied more completely, the LHS typically increases in metamorphic grade structurally upward from greenschist (chlorite zone) at its lower MBT boundary through the garnet zone (**Figure 2a**) to middle amphibolite facies (staurolite/kyanite zone) at its upper MCT boundary. A clear lithologic change usually defines the MCT, but this happens to nearly coincide with the kyanite isograd in many sections (Le Fort 1975). The upward increase in metamorphic grade continues within the GHS, which typically ranges from middle amphibolite facies (kyanite zone) at the MCT (**Figure 2b**) to lower granulite facies (sillimanite–K-feldspar, cordierite, and spinel anatectites; locally orthopyroxene-bearing metabasites) in its metamorphic core, where partial melts are common (**Figure 2c,d**). In some sections, the STDS truncates GHS isograds at upper amphibolite to granulite facies, but in others, a continuous decrease in metamorphic grade occurs at the top of the GHS (**Figure 2e**). The THS typically decreases in metamorphic grade from middle or lower amphibolite facies at its lower STDS contact to unmetamorphosed structurally upward.

Figure 3 illustrates typical metamorphic patterns in the northwestern, central, and eastern Himalaya. The MCT and STDS demarcate the LHS-GHS-THS boundaries. In the Zanskar region of northwestern India (**Figures 1** and **3a**), sub-garnet-zone LHS rocks are exposed in the Kishtwar Window (KW), with rapid increases to kyanite- and sillimanite-zone lower GHS rocks structurally upward (e.g., Walker et al. 2001). A more gradual increase to the sillimanite–K-feldspar zone occurs within the GHS, with a rapid decrease in metamorphic grade to sub-garnet-zone GHS and THS rocks near the STDS, which extensionally thins and truncates metamorphic isograds (e.g., Walker et al. 2001). To the south, however, in the Rampur Window (RW) region, no truncation or telescoping of metamorphic zones is observed at the GHS-THS contact, and the STDS may have little displacement or be absent altogether. Central Nepal (**Figure 3b**) also shows a continuous increase in metamorphic grade structurally upward within the LHS and GHS (see Pêcher 1989). A rapid decrease in metamorphic grade within the THS is spatially associated with the STDS (Schneider & Masch 1993). Indeed, the central Nepal section (**Figure 3b**) has long served as the paradigm of Himalayan metamorphism (Le Fort 1975). In central Bhutan (**Figure 3c**), although a rapid increase in metamorphic grade occurs across the MCT (Daniel et al. 2003, Long & McQuarrie 2010), some metamorphic features differ in comparison with other sections. For example, garnet-zone THS rocks occur in a downwarped syncline in the
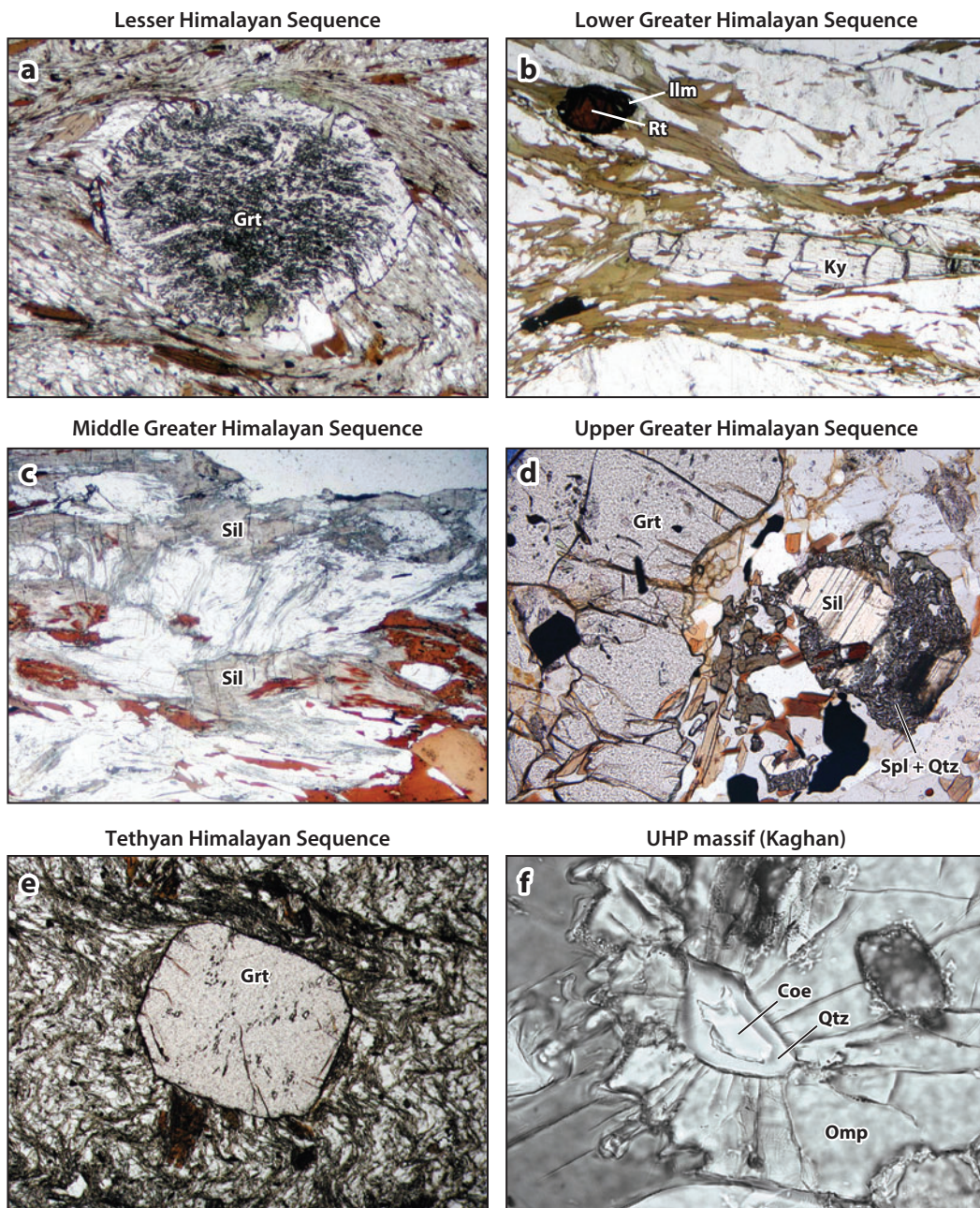
Figure 2

Photomicrographs of typical Himalayan metamorphic rocks. (*a–c*) Central Nepal Grt-grade Lesser Himalayan Sequence, Ky-grade structurally lower Greater Himalayan Sequence, and Sil-Kfs-grade structurally higher Greater Himalayan Sequence. (*d*) High-grade Greater Himalayan Sequence from Sikkim showing Spl + Qtz symplectites overprinting Sil + Bt. Adapted from Rubatto et al. (2013) with kind permission from Springer Science and Business Media. (*e*) Grt-grade Tethyan Himalayan Sequence from central Bhutan. (*f*) Omphacite from Kaghan ultrahigh-pressure eclogite with inclusion of coesite that has partially reacted to quartz (modified from O'Brien et al. 2001). Abbreviations: Bt, biotite; Coe, coesite; Grt, garnet; Ilm, ilmenite; Kfs, K-feldspar; Ky, kyanite; Omp, omphacite; Qtz, quartz; Rt, rutile; Sil, sillimanite; Spl, spinel.
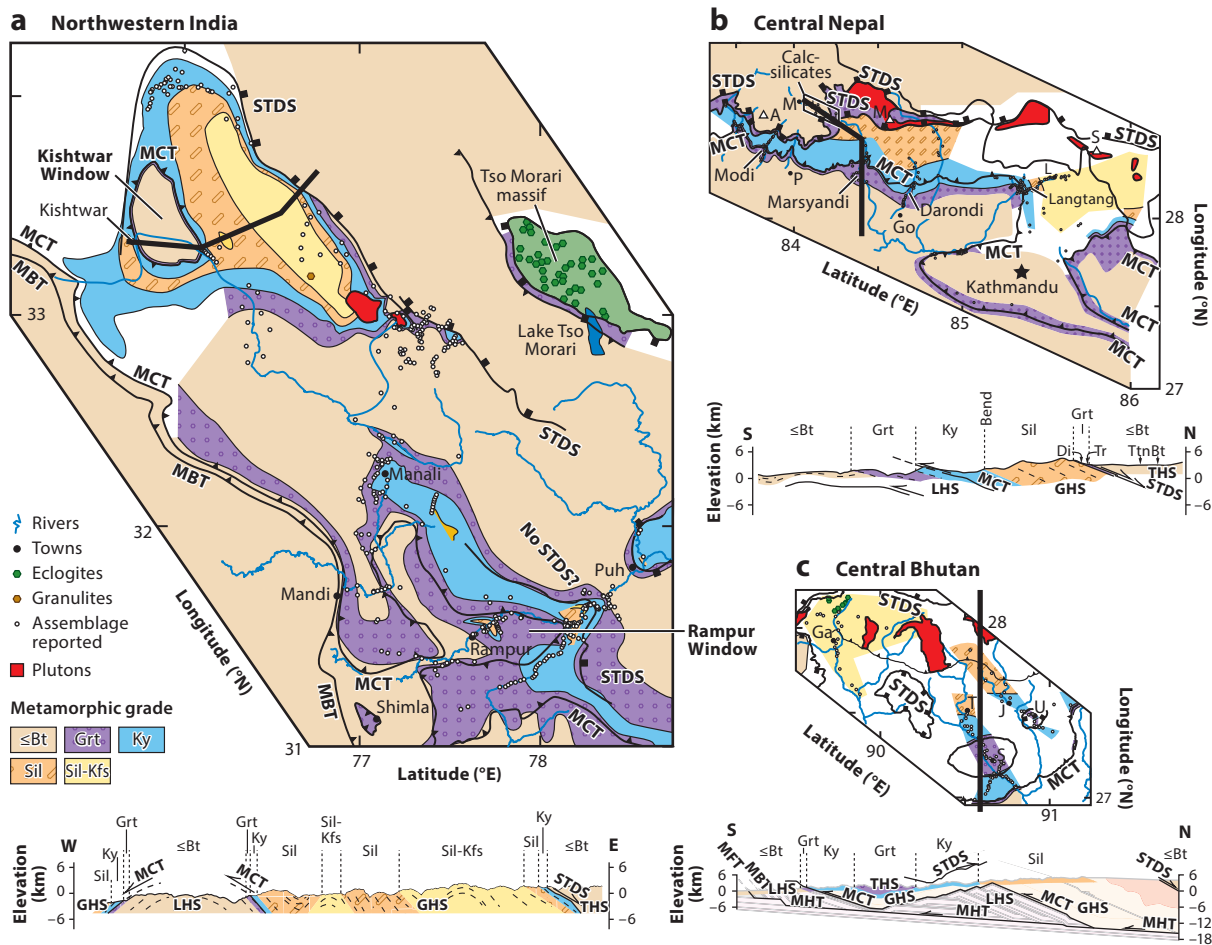
Figure 3

Metamorphic maps and cross sections illustrating high-grade GHS rocks sandwiched between lower-grade LHS and THS rocks. Heavy black lines show cross-section locations. (*a*) Northwestern India. (*b*) Central Nepal. (*c*) Central Bhutan. The STDS truncates or telescopes isograds in northwestern India and central Nepal, whereas metamorphic grade changes smoothly from GHS to THS in the Shemgang region of central Bhutan. See **Supplemental Material** for references. Geologic abbreviations: GHS, Greater Himalayan Sequence; LHS, Lesser Himalayan Sequence; MBT, Main Boundary Thrust; MCT, Main Central Thrust; MHT, Main Himalayan Thrust; STDS, South Tibetan Detachment System; THS, Tethyan Himalayan Sequence. Mineralogic abbreviations: Bt, biotite; Di, diopside; Grt, garnet; Kfs, K-feldspar; Ky, kyanite; Sil, sillimanite; Tr, tremolite; Ttn, titanite. Mountains: A, Annapurna; M, Manaslu; S, Shishapangma. Towns: Ga, Gasa; Go, Ghorka; J, Jakar; L, Langtang; M, Manang; P, Pokhara; S, Shemgang; T, Trongsa; U, Ura.

▶ Supplemental Material

Shemgang region but show no obvious metamorphic discontinuities adjacent to the GHS (Long & McQuarrie 2010, Corrie et al. 2012). Moreover, the GHS shows dip- or transport-parallel changes in metamorphic grade: Sillimanite-zone or even sillimanite–K-feldspar-zone rocks occur toward the hinterland, whereas only kyanite-zone rocks occur toward the foreland (Swapp & Hollister 1991, Long & McQuarrie 2010). This across-strike pattern may be common: Outliers near Shimla in northwestern India (**Figure 3a**) and Kathmandu in central Nepal (**Figure 3b**) are lower grade than their putative hinterland counterparts, but stratigraphic and structural continuity with across-strike GHS rocks is less assured.

Even this brief discussion illustrates several prominent features of Himalayan metamorphism. First, along-strike consistency is truly amazing: The LHS-GHS-THS units exhibit consistent metamorphic grades over distances approaching 2,000 km. Second, metamorphic grade is consistently inverted from the LHS through the GHS, again along a strike length of approximately 2,000 km. Last, the STDS commonly telescopes or truncates metamorphic grade from the top of the GHS through the base of the THS. All these facts have ignited intense debate over the tectonic drivers of Himalayan metamorphism and, conversely, the insights that Himalayan metamorphic rocks provide into collisional tectonics. Common questions include the following: Did thrusting along the MCT drive inverted metamorphism between its hanging wall and footwall and if so, how? How do partial melting and high erosion rates influence metamorphic and tectonic evolution? Was extensional shear along the STDS a short-lived event, or was it long lasting and crucial for controlling exposure of the high-grade Himalayan core?

Local metamorphic anomalies punctuate this broad backdrop. Ultrahigh-pressure (UHP) eclogites near the Nanga Parbat syntaxis and at Tso Morari in the northwest Himalaya, dated at 45–55 Ma (e.g., de Sigoyer et al. 2000, Kaneko et al. 2003) (**Figure 2f**), have sparked debate regarding early deep metamorphism. Granulite-facies overprinting of young eclogites ($\leq \sim 25$ Ma; Corrie et al. 2010) from eastern Nepal to western Bhutan has similarly fostered discussion regarding pressure-temperature (P-T) evolution of deeply buried rocks and mechanisms for high-T exhumation during the latter half of the orogen's evolution. Last, the Nanga Parbat and Namche Barwa syntaxes expose young (≤ 25 Ma) granulite-facies rocks and possibly reflect complex interaction among structural evolution, partial melting reactions, and focused erosion (Zeitler et al. 2001b).

THERMOBAROMETRY: QUANTIFYING THE METAMORPHIC INVERSION

Models of the development of the Himalayan orogenic wedge depend on the conditions of metamorphism and distributions of peak metamorphic pressure (P) and temperature (T). Strenuous efforts—over 100 publications—have been exerted to quantify Ps and Ts. Although one might like to plot all data for a region together, unfortunately over half of these studies employed improper petrologic practice or simply did not provide sufficient documentation to permit critical evaluation of results (Kohn & Spear 2000; see sidebar, What Makes a Good Metamorphic Study?). In addition, different studies used different approaches, as follows:

1. Conventional thermobarometry solves a small number of specific calibrated equilibria, usually the Grt-Bt or Grt-Hbl Fe-Mg exchange thermometers and the Grt-Pl-Ms-Bt, Grt-Pl-Hbl-Qtz, or Grt-Pl-Alsi-Qtz barometers. Trace element and spectroscopic thermometers are now increasingly used (e.g., Beyssac et al. 2004, Kohn 2008, Corrie et al. 2010). Advocates argue that we know the thermodynamics of these equilibria best, permitting the most accurate P-T estimates. Critics argue that a single wrong composition can produce implausible results and that this approach does not evaluate whole-rock equilibration.

2. Multiequilibrium thermobarometry solves a large number of equilibria within the context of an internally consistent thermodynamic database, usually Thermocalc's average P-T algorithm (Powell & Holland 1994). Thermocalc propagates errors in thermochemical properties including assumed uncertainties in the activities of each mineral component, regardless of the actual chemical heterogeneity observed in a mineral, which may be substantially better or worse. Advocates argue that if a rock is well equilibrated, then all equilibria should return

UHP: ultrahigh-pressure; UHP metamorphic rocks contain coesite or diamond

Grt: garnet

Bt: biotite

Hbl: hornblende

Pl: plagioclase

Ms: muscovite

Qtz: quartz

Alsi: aluminosilicate (andalusite, kyanite, or sillimanite)

WHAT MAKES A GOOD METAMORPHIC STUDY?

I consider the following 5 factors:

1. Good geologic practice. Are samples located? Are mineral assemblages reported? Does textural documentation help interpret reactions and selection of petrologically relevant compositions? Numerous studies do not report mineral assemblages (see distribution of samples versus mineral zones in **Figure 3**) or occasionally even sample locations, and many pro forma textural descriptions do not advance petrologic interpretations.

2. Analytical quality. Are full analyses provided, are anhydrous minerals (garnet, plagioclase, pyroxene) stoichiometric to within 1–2%, and are wt% totals within expected ranges? On an anhydrous basis, wt% totals are typically 94–96% for muscovite, 95–97% for biotite, 96.5–98.5% for amphiboles, 99–101% for feldspars and pyroxenes, and 99–102.5% for garnet. A few suspect analyses do not indict an entire study but should be rare. Some computational programs warn against compositions that fail stoichiometric and wt% criteria (e.g., Program Thermobarometry; Spear et al. 1991).

3. Characterization of compositional zoning. Were X-ray maps of major and minor elements collected for garnet and other key minerals? Garnet compositions form the foundation of most quantitative interpretations, which in turn require understanding spatial distributions of chemistry (e.g., see Spear 1993, Kohn 2013). Whereas detailed line-traverses (typically 100 or more points across individual grains) have been employed since the late 1980s to characterize garnet zoning, X-ray maps first became common in the early to mid-1990s, prior to 80–90% of publications on Himalayan metamorphism. Compositional zoning in plagioclase can be imaged directly using backscattered electrons (BSE), but X-ray maps or spot-to-spot analyses may be required to characterize other minerals or trace element variations. For chemically zoned or heterogeneous minerals, where do reported compositions fall on X-ray maps or within the spectrum of compositions?

4. Petrologic criteria. What (if any) petrologic criteria were employed in selecting compositions? For example, how do reported compositions correspond to petrologic models of how chemical zoning forms (e.g., see Tracy et al. 1976, Spear et al. 1990, Spear 1993, Kohn & Spear 2000)? For calculating P-T conditions, were corrections made for retrograde reactions (Kohn & Spear 2000)?

5. Consistency with phase equilibria. Are reactions, P-T conditions, and P-T paths consistent with mineral stability fields, especially in metapelites where petrogenetic grids are well established?

Typical good studies use WDS (wavelength dispersive spectrometry, a precise electron beam method) analysis for major, minor, and more abundant trace elements (e.g., Zr in rutile), or LA-ICP-MS (laser-ablation, inductively coupled plasma mass spectrometry, a highly precise method for determining trace element concentrations and U-Th-Pb age) or ion microprobe analysis for trace elements standardized to the same mineral (a rutile standard for rutile, a titanite standard for titanite, etc.). They also include composition maps and explain how compositions were chosen for quantitative interpretations based on petrologic criteria, applying compositional corrections as needed. Less compelling studies do not illustrate zoning or explain where compositions were collected (e.g., simply reporting "rim" compositions), do not identify any petrologic criteria for selecting compositions, infer results that contradict phase equilibria, and/or have nonstoichiometric analyses [commonly but not ubiquitously from EDS (energy dispersive spectrometry, a less precise electron beam method for analyzing major and minor elements)]. These criteria eliminate numerous thermobarometric and P-T path studies from consideration. For example, of 107 thermobarometric studies considered for this review, a majority (61) failed at least one (usually several) of these criteria and could not be interpreted quantitatively.

the same P-T condition. Critics argue that many equilibria are sensitive to parameters that are difficult to constrain, such as H_2O activity or mixing properties, leading to erroneous P-T estimates, and that some well-calibrated equilibria—such as highly temperature sensitive Fe-Mg exchange reactions—are not considered.

3. Pseudosection (bulk-composition-specific phase diagram) analysis delineates mineral assemblage stability fields and now commonly also contours fields for mineral compositions. Advocates argue that, if phase equilibrium constraints are the final arbiter of thermobarometric accuracy (see sidebar, What Makes a Good Metamorphic Study?), then we should just calculate and use phase equilibrium constraints. Critics argue that these diagrams often make untestable assumptions about whole-rock reactivity and mineral compositional homogeneity.

Largely because of the sensitivity of method 2 to H_2O activity, some practitioners use a specific thermometer, usually Grt-Bt Fe-Mg exchange, to constrain T, while using multiple equilibria to solve for P and H_2O activity—essentially a hybridization of methods 1 and 2 (e.g., Stephenson et al. 2000). Others use Thermocalc to determine P and T for specific thermometers and barometers (Webb et al. 2011)—essentially method 1, except with Thermocalc's thermodynamics.

To ensure greatest thermobarometric compatibility, I recalculated P-T conditions for approximately 300 rocks that passed quality control criteria in four areas across the Himalaya (**Figure 1**) using an internally consistent set of thermobarometric equilibria (see **Supplemental Material**; follow the **Supplemental Material link** from the Annual Reviews home page at **http://www.annualreviews.org**), especially emphasizing P-T distributions across the MCT and STDS. Key features (**Figure 4**) include the following:

▶ Supplemental Material

1. Temperatures. All regions show sharp but continuous increases across the MCT from T ≈ 550°C in the LHS to T = 700–800°C in the GHS (**Figure 4m**). Stability of Ky + Bt occurs at T ≈ 600°C (Spear & Cheney 1989), which explains why the kyanite isograd commonly occurs near the MCT: The gradient is consistently steep over a range of Ts that includes 600°C. Metapelites and metasammites experience muscovite dehydration melting at T ≥ 700°C (e.g., Spear et al. 1999), and calculated Ts above this in the GHS core explain the common occurrence of migmatites there as well as with occurrences of cordierite and orthopyroxene expected at T ≥ 750°C (Spear et al. 1999, Pattison et al. 2003). The steepest gradients are documented in Bhutan (**Figure 4j**) and in the densely sampled central Kumaun to Langtang sector (**Figure 4d**), where a consistent T profile is observed along strike for ~700 km. Raman spectroscopic data for low-grade LHS in Kumaun (**Figure 4d**) and THS at Everest (**Figure 4g**) show smooth, moderately to very steep decreases in T; Raman data in Bhutan (**Figure 4j**) suggest a similar pattern but are too scattered to resolve gradients independently.

2. Pressures. Most transects show a steep increase in P across the MCT (**Figure 4n**), again with the largest and most consistent step in the Kumaun to Langtang sector (**Figure 4e**). Steeper than lithostatic (superlithostatic) P gradients above the MCT occur at Kumaun (India), Langtang (Nepal), and Shemgang (Bhutan; **Figure 4e,k**), but lithostatic gradients occur in both northwestern India and the upper reaches of Langtang (**Figure 4b,e**). Although data are few, the lack of an anomalous P or T gradient or discontinuity across the GHS-THS contact in northwestern India suggests that the STDS has substantially less displacement than, for example, in the Everest region or Bhutan.

3. Combined P-T conditions. Most rocks plot within the kyanite stability field (**Figure 4o**), but rocks from Nyalam to Sikkim and the structurally highest rocks at Langtang plot well within the sillimanite stability field (**Figure 4f,i**). This result implies an absence of anomalous heat sources for much of the metamorphic wedge, but reliable thermobarometric data are
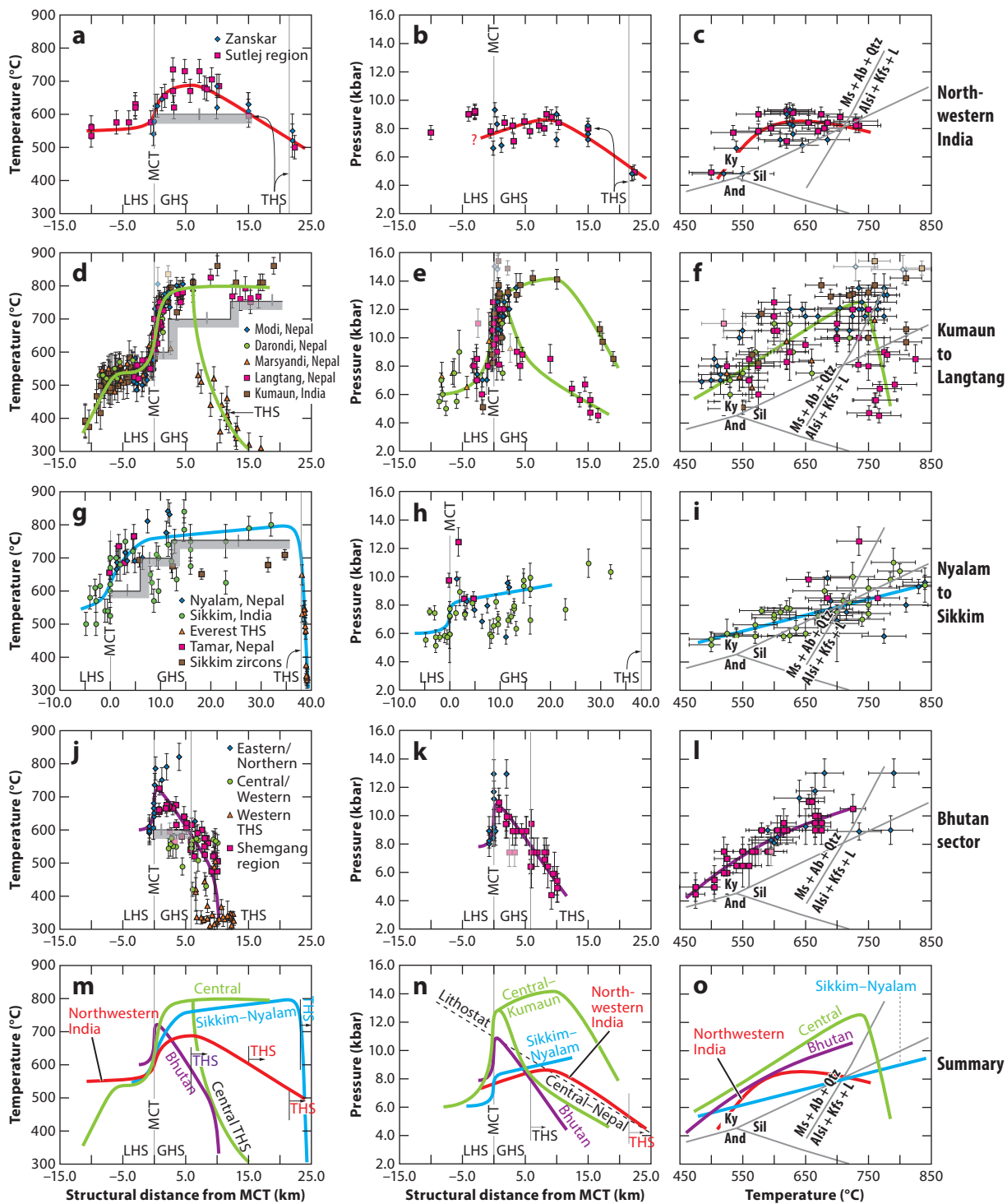
sparser for higher-grade rocks. At structurally high levels of the GHS, high Ts and low Ps increasingly prevail.

PRESSURE-TEMPERATURE PATHS OF THE METAMORPHIC SANDWICH

Pressure-temperature (P-T) paths are most commonly determined using one of three thermodynamically based methods: differential thermodynamics, pseudosection analysis, and petrogenetic grids (phase diagrams that apply over a range of bulk compositions). A key thermodynamic concept is that mineralogy and mineral compositions in a rock reflect a particular P and T (Duhem's theorem). Sufficiently large changes to P and T (ΔP and ΔT, respectively) will stabilize different assemblages, whereas smaller ΔP and ΔT within the stability field of a single assemblage drive changes to mineral abundances and compositions. If ΔP and ΔT cause a garnet to grow, and intracrystalline diffusion is not too fast, then the garnet will encode a series of equilibrium compositions from core to rim. The exact form of such zoning depends on ΔP, ΔT, and the mineral assemblage.

In principle P-T paths can be calculated for many rock types, but tectonic applications commonly emphasize ΔP or the P-T path trajectory because this distinguishes better among tectonic models than does ΔT alone (e.g., Spear et al. 1984). In the amphibolite facies, P and ΔP estimates depend principally on Ca partitioning between garnet and compositionally intermediate plagioclase (typically $0.15 < X_{An} < 0.60$). Although amphibolite-facies P-T paths are sometimes calculated for plagioclase-absent rocks, these do not normally resolve ΔP well and should be avoided for thermodynamic calculations.

Most applications of differential thermodynamics assume a mineral assemblage and invert chemical zoning in garnet and plagioclase to determine the ΔP and ΔT over which the garnet grew. This approach uses the differential forms of thermodynamic equations to relate changes in mole fraction (ΔX) to ΔP and ΔT. Its main advantage is that it requires relatively few assumptions about mineral equilibration (only mineral rims need equilibrate) or changes to whole-rock chemistry. However, this method presumes a mineral assemblage and can be severely biased at higher temperatures by diffusional modification of compositions (Florence & Spear 1991)—for example, erroneously implying isothermal decreases in pressure. Thus, it is most reliable for LHS and THS rocks with relatively simple lower amphibolite-facies Grt + Bt + Chl assemblages and is impracticable in most high-grade GHS garnets whose compositional zoning complexly reflects multiple reactions plus diffusional modification.

Pseudosection analysis takes specific whole-rock compositions, typically from X-ray fluorescence analysis or point counting, and, using mass balance constraints and integrated thermodynamic expressions, calculates the P-T distribution of mineral assemblage stability fields and mineral compositions within each field. Mass balance constraints reduce thermodynamic variance to 2 (Duhem's theorem), so in principle, a single garnet composition with two or more independent Xs can be linked with a P-T condition and mineral assemblage in which that garnet formed.

←——

Figure 4

Thermobarometric transects from western through eastern Himalaya quantify temperature and pressure versus structural distance, and pressure versus temperature arrays. See **Figure 1** for locations. (*a–c*) Northwestern sector. (*d–f*) Central sector. (*g–i*) East-central sector. (*j–l*) Bhutan sector. (*m–o*) Summary of trends. Gray bars show petrogenic limits on temperature. Geologic abbreviations: GHS, Greater Himalayan Sequence; LHS, Lesser Himalayan Sequence; MCT, Main Central Thrust; THS, Tethyan Himalayan Sequence. Mineralogic abbreviations: Ab, albite; Alsi, aluminosilicate; And, andalusite; Kfs, K-feldspar; Ky, kyanite; L, liquid; Ms, muscovite; Qtz, quartz; Sil, sillimanite.

Multiple garnet compositions can be used to infer a P-T path. Alternatively, a series of mineral assemblages as determined from inclusions can be linked to their respective regions in P-T space to derive a P-T path. This method's main advantage is that it has a low thermodynamic variance and requires less compositional correlation. However, it requires more assumptions about mineral equilibration (commonly, minerals are assumed to be compositionally homogeneous and completely equilibrated). Thus, arguably, pseudosection analysis may be preferred for high-grade GHS rocks, where high T ensures a closer approach to whole-rock equilibrium, but avoided at low T, where complete mineral equilibration is unlikely. At high T, however, diffusional modification of garnet compositions must be addressed.

Petrogenetic grids effectively map out the occurrences of major reactions in P-T space. Although similar to pseudosections, grids apply over a broader region of composition space, relaxing assumptions about whole-rock equilibration. Usually a series of mineral textures is used to identify a sequence of reactions that constrains the P-T evolution. This approach can be applied to mutually proximal rocks that preserve different reaction textures or to a single rock with multiple textures.

Petrogenetic grids form the basis of several P-T path estimates, but different grids can yield different interpretations. For example, Swapp & Hollister (1991) and Davidson et al. (1997) used textures and reaction topologies of H_2O-saturated grids to infer nearly isothermal high-T exhumation of GHS rocks in Bhutan (**Figure 5a**). Most importantly, occurrences of cordierite and spinel were thought to require P ≤ 4 kbar at T ≥ 750°C (**Figure 5a**). Such low Ps ultimately led to the channel flow concept (Grujic et al. 1996), but contrast markedly with thermobarometric arrays (albeit typically at lower grades; **Figure 4**). More relevantly, for two reasons, partial melting reactions and mineral activities <1 strongly affect textural and P-T path interpretations. First, partial melts are inevitable in these rocks, and reactions to produce cordierite in melt-present grids are much more temperature sensitive than in melt-absent grids (Spear et al. 1999) (**Figure 5a,b**). Second, spinel-forming reactions depend sensitively both on quartz activity [a(Qtz)] and on additional mineral components, particularly gahnite (Zn-spinel; Waters 1991). Spinel in many GHS rocks contains Zn and is not associated with quartz [so commonly a(Qtz) < 1, although see Neogi et al. (1998) and Rubatto et al. (2013) (**Figure 2e**) for important textural counterexamples]. Both factors displace the main spinel-forming reaction to higher P (**Figure 5b**). Thus, although spinel and cordierite could still have formed at P ≤ 4 kbar, many occurrences could alternatively have

→

Figure 5

P-T paths calculated for main belt of LHS-GHS-THS rocks. (*a,b*) H_2O-saturated (melt-absent) grid (Davidson et al. 1997; modified with permission from Wiley-Blackwell) and melt-present petrogenetic grid (Spear et al. 1999; modified with permission from Springer) for metapelitic compositions with possible P-T paths (*gray arrows*). Light blue shading shows regions of H_2O saturation. Other shading shows regions of staurolite, cordierite, spinel, and orthopyroxene stabilities. Reaction textures for high-grade rocks in Bhutan in the context of the H_2O-saturated petrogenetic grid suggest nearly isothermal high-T exhumation (Swapp & Hollister 1991, Davidson et al. 1997) but could possibly be explained by isobaric heating and cooling in grids that include partial melting (Spear et al. 1999). Bright white stars show maximum P-T locations of Crd-Spl assemblages; dull white stars show corresponding locations from the alternative grid. Location of the spinel-forming reaction is sensitive to additional components (Waters 1991) and SiO_2 activity.
(*c*) P-T paths from LHS and THS rocks in northwestern India, central Nepal, and central Bhutan as calculated using differential thermodynamics (Kohn et al. 2001, 2004; Kohn 2004; Corrie et al. 2012). (*d,e*) Pseudosections and P-T paths calculated from garnet compositions in migmatitic rocks from the Everest region of eastern Nepal (Groppo et al. 2012), ignoring melt loss (*d*) or reintegrating melt (*e*). AE Gran and AE Amph refer to granulite- and amphibolite-facies overprinting P-T conditions for Arun (eastern Nepal) eclogites from the same structural level (Corrie et al. 2010). Geologic abbreviations: GHS, Greater Himalayan Sequence; LHS, Lesser Himalayan Sequence; THS, Tethyan Himalayan Sequence. Mineralogic abbreviations: Ab, albite; Alsi, aluminosilicate; And, andalusite; Bt, biotite; Chl, chlorite; Crd, cordierite; Grt, garnet; Ilm, ilmenite; Kfs, K-feldspar; Ky, kyanite; L, liquid; Ms, muscovite; Pl, plagioclase; Opx, orthopyroxene; Qtz, quartz; Rt, rutile; Sil, sillimanite; Spl, spinel; St, staurolite. Other abbreviations: KFMASH, K_2O-FeO-MgO-Al_2O_3-SiO_2-H_2O; NaKFMASH, Na_2O-K_2O-FeO-MgO-Al_2O_3-SiO_2-H_2O.

formed at ∼800°C and ∼7 kbar (**Figure 5b**), similar to peak P-T conditions inferred elsewhere in the GHS (**Figure 4**).

Differential thermodynamics–based P-T paths have been calculated for central Nepal Grt-grade LHS (Kohn et al. 2001, 2004; Kohn 2004), eastern Nepal LHS and GHS (Imayama et al. 2010), and Bhutan Grt-grade THS (Corrie et al. 2012). The assumed assemblages in Imayama et al.
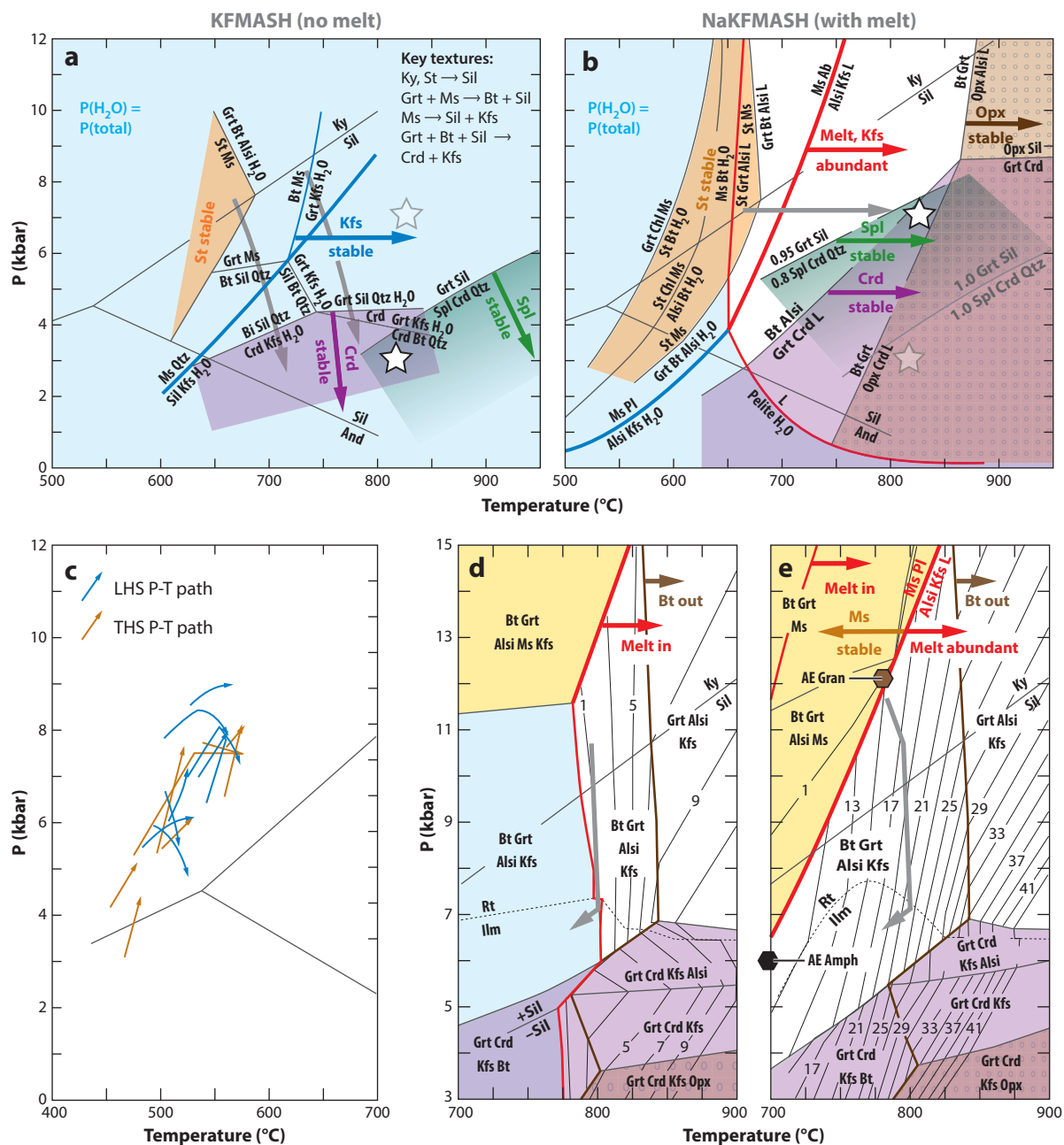
(2010), particularly coexistence of rutile and ilmenite, contrast with observed textures, so although calculated paths compare well with other studies, they are not presented here. Detailed data from Chambers et al. (2009) permit semiquantitative calculations (see **Supplemental Material**). All P-T paths (**Figure 5c**) occupy a restricted region of P-T space and show small ΔTs but various ΔPs, including simple loading (monotonic increases in P and T), loading followed by isobaric heating, and exhumation with heating. Comparable paths are observed in both the LHS and THS, although THS paths that explicitly show exhumation with heating are not yet identified. These paths generally imply that metamorphism accompanied thrust loading (no surprise), but the relatively small ΔTs and restriction to the kyanite stability field generally exclude extraneous heat sources or protracted heating following thrusting.

Pseudosection-based P-T paths in the Himalaya were first calculated for upper amphibolite-facies GHS rocks in northwestern India (Vance & Mahar 1998), and numerous published examples now range over all geographic sectors from the lower amphibolite to granulite facies. Few such calculations address issues of whole-rock reactivity, however, which can dramatically affect which mineral assemblages are stable, their location in P-T space, and the compositions of their constituent minerals (e.g., Spear et al. 1990, Gaidies et al. 2008). For example, it has long been known that Ca zoning in garnet depends on the reactivity of other calcic phases (e.g., Menard & Spear 1993), so that ΔP cannot be determined reliably from ΔX_{Ca} alone (Spear et al. 1990). This is one reason why differential thermodynamic P-T path calculations rarely employ mass balance constraints and instead emphasize garnet and plagioclase compositional correlation. Chemical zoning in other minerals (e.g., amphibole, pyroxene, mica) and epitaxial or coronitic textures further attest to incomplete whole-rock equilibration. For example, Lanari et al. (2013) reported that mineral reactions in the Stak eclogite do not reflect the whole-rock composition, and they instead recommend use of local compositional subdomains for pseudosection interpretation.

In contrast to most pseudosection-based studies, Groppo et al. (2010, 2012, 2013) directly addressed issues of whole-rock compositional change due to melt loss in their analysis of migmatites in the Everest region of eastern Nepal (see also Guilmette et al. 2011 for Namche Barwa syntaxis core rocks). These rocks are amenable to pseudosection modeling because high T promotes whole-rock equilibration. Models (**Figure 5d,e**) show that although melt loss does not significantly shift the P-T locations of cordierite- and orthopyroxene-bearing assemblages, it profoundly affects calculated melt production and the location of muscovite- and biotite-bearing assemblages. Basically, reintegrating melt components predicts topologies more similar to petrogenetic grids. For example, both predict major melt production across the muscovite dehydration-melting reaction, which textures and geochemistry indicate was a key leucogranite-producing reaction in the Himalaya (Inger & Harris 1992, Harris & Massey 1994). The pseudosection-based P-T paths as determined from garnet chemistry (Groppo et al. 2012) (**Figure 5d,e**) show nearly isothermal exhumation, qualitatively similar to the path inferred in Bhutan (Swapp & Hollister 1991, Davidson et al. 1997) but displaced to higher P. The path determined by Groppo et al. fits neatly into bounding P-T conditions determined thermobarometrically from granulite- and amphibolite-facies overprinting assemblages of eclogites from a similar structural position (Corrie et al. 2010) (**Figure 5e**).

ECLOGITES AND ECLOGITES

Two general occurrences of eclogites are found in the Himalaya: (*a*) ∼50 Ma UHP and near-UHP eclogites in Pakistan (Kaghan and Stak) and northwestern India (Tso Morari), and (*b*) ∼25 Ma HP eclogites distributed from eastern Nepal and southern Tibet through western Bhutan. These two groups are distinguished on the basis of metamorphic P-T conditions, ages, and (inferred)

mechanisms of formation and exhumation (e.g., see Lombardo & Rolfo 2000, Guillot et al. 2008). With some notable exceptions (e.g., Lanari et al. 2013, St-Onge et al. 2013), P-T paths for these rocks are typically determined by calculating specific P-T conditions for peak eclogite versus overprinting assemblages and connecting these points through P-T space. The highest-P eclogites for a region are emphasized here.

In the northwestern Himalaya, eclogites were first discovered ca. 1950 (Berthelsen 1953), then rediscovered ca. 1990 (e.g., Pognante & Spencer 1991, Pognante et al. 1993, Guillot et al. 1995). Within a decade, UHP conditions (presence of coesite) were documented for Kaghan and Tso Morari (Mukherjee & Sachan 2001, O'Brien et al. 2001, Kaneko et al. 2003) (**Figure 2f**). The eclogites occur as boudinaged, metamorphosed, mafic dikes in thrust slices assigned to the GHS and THS along the leading edge of the Indian subcontinent (e.g., see Kaneko et al. 2003, Treloar et al. 2003, de Sigoyer et al. 2004, Guillot et al. 2008, Lanari et al. 2013).

Peak P-T conditions are principally based on Grt chemistry and thermobarometry of Grt + Cpx + phengite assemblages, and are consistent with the presence of coesite in the Kaghan and Tso Morari eclogites (Kaneko et al. 2003, Rehman et al. 2007, Wilke et al. 2010a, St-Onge et al. 2013), and with an absence of coesite in the Stak eclogites (Lanari et al. 2013) (**Figure 6a**). All eclogites record exhumation by 15–20 kbar. P-T conditions of surrounding felsic gneisses and
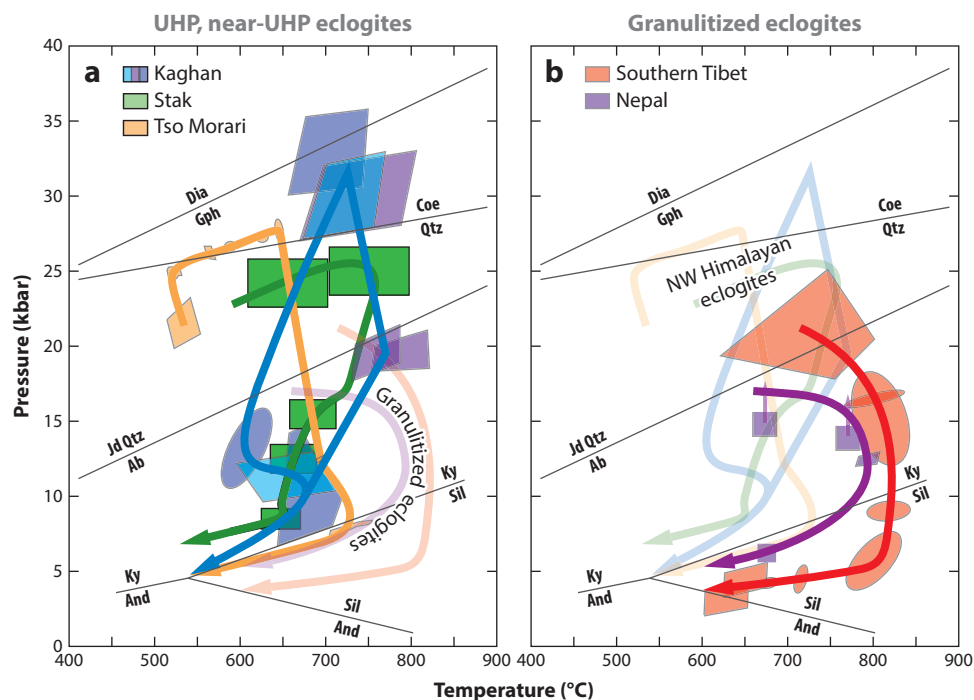

Figure 6

P-T paths (*arrowed lines*) for Himalayan eclogites (Kaneko et al. 2003, Groppo et al. 2007, Corrie et al. 2010, Wilke et al. 2010a, Lanari et al. 2013, St-Onge et al. 2013). Boxes and ellipses represent specific P-T constraints (minimum P limits in one case). Light P-T paths duplicate corresponding paths for the other eclogite type for comparison. (*a*) Ultrahigh-pressure (UHP) and near-UHP rocks from India and Pakistan. (*b*) Granulitized eclogites from southern Tibet and eastern Nepal. Reference univariant reactions are from Hemingway et al. (1998; Qtz-Coe), Holland (1980; Ab-Jd-Qtz), Pattison (1992; Ky-Sil-And), and Day (2012; Dia-Gph). Abbreviations: Ab, albite; And, andalusite; Coe, coesite; Dia, diamond; Gph, graphite; Jd, jadeite; Ky, kyanite; Qtz, quartz; Sil, sillimanite.

comparisons among different eclogites suggest heating of some Tso Morari and Kaghan eclogites during exhumation (Rehman et al. 2007, St-Onge et al. 2013), whereas a blueschist overprint suggests initial cooling of a Kaghan eclogite (Wilke et al. 2010a; see also Lombardo et al. 2000 for inferred quasi-isothermal exhumation) (**Figure 6a**). Kaghan and Tso Morari eclogites record subsequent heating at moderate pressure; e.g., hornblende overprints glaucophane in the Kaghan eclogite and Hbl-Pl Ts are ~675°C (Wilke et al. 2010a) (**Figure 6a**). Lower-P paths exhibiting nearly isothermal exhumation with a moderate-P thermal overprint have been inferred from Tso Morari (de Sigoyer et al. 1997, Guillot et al. 1997).

Focusing on ages that can be linked definitively to metamorphic conditions, the Kaghan eclogites are best studied, with a Grt-Cpx Sm-Nd age of 49 ± 12 Ma, U-Pb ages on zircon domains with quartz versus coesite inclusions of ~50 versus 46.2 ± 0.7 Ma, $^{40}Ar/^{39}Ar$ ages for phengite and hornblende of ~47 Ma, cooling ages for rutile (U-Pb) and phengite (Rb-Sr) of 39–44 Ma, and apatite fission track and U-Th/He ages as old as 20–25 Ma (Tonarini et al. 1993; Kaneko et al. 2003; Treloar et al. 2003; Wilke et al. 2010b, 2012). Most notably, the age of eclogitization (46–47 Ma; U-Pb on zircon with coesite inclusions and $^{40}Ar/^{39}Ar$ on phengite) closely follows initial collision (50–55 Ma; Najman et al. 2010), with a rapid transition to posteclogite facies overprinting and cooling (44–47 Ma; $^{40}Ar/^{39}Ar$ on hornblende, U-Pb on rutile, and Rb-Sr on phengite). The latter data imply exhumation rates up to 100 km/Myr (Wilke et al. 2010b). Data from Tso Morari include Lu-Hf and Sm-Nd ages on eclogitic garnets of 55 ± 12 and 55 ± 7 Ma, U-Pb ages on zircon inclusions in a garnet core of 58 ± 2 Ma and in garnet rims of 46 ± 3 Ma, $^{40}Ar/^{39}Ar$ and Rb-Sr ages on phengite of 48–54 and 46 ± 4 Ma, and zircon fission track ages of 34–45 Ma (de Sigoyer et al. 2000, Schlup et al. 2003, Donaldson et al. 2013, St-Onge et al. 2013), also suggesting rapid transitions from the initiation of collision to peak eclogitization and thence to exhumation and cooling in the mid- to upper crust.

Eclogites with a strong granulite- to amphibolite-facies overprint were first discovered in southern Tibet near Everest in the late 1990s (Lombardo & Rolfo 2000) and occur as metamorphosed boudinaged mafic dikes. Virtually identical rocks are described in eastern Nepal and northwestern Bhutan (e.g., Corrie et al. 2010, Grujic et al. 2011) (**Figure 1**). The following discussion of the Nepal/Tibet eclogites is based on Lombardo & Rolfo (2000), Groppo et al. (2007), Cottle et al. (2009), and Corrie et al. (2010). Garnet composition maps and inclusion textures indicate that granulite-facies rims overgrew eclogite-facies cores. Matrix orthopyroxene and Opx + Pl symplectites attest to late-stage granulite-facies conditions, whereas matrix hornblende replaces pyroxenes and indicates a latest-stage amphibolite-facies overprint. Omphacite sensu stricto is not preserved (maximum jadeite contents of inclusions in garnet are ~15%). Rather, diopsidic matrix pyroxene is either surrounded by or intergrown with plagioclase that is interpreted to have exsolved from HP omphacite with jadeite contents up to 30–40%. Reintegrated omphacite compositions, Zr-in-Ttn thermometry, and various overprinting assemblages constrain P-T paths, which record peak conditions at higher T and lower P than for the northwestern Himalayan eclogites (**Figure 6b**); i.e., these paths indicate greater heating in the middle crust.

Eclogitization has not been dated directly, but a Lu-Hf garnet age of 20.7 ± 0.4 Ma represents a mixture of eclogite-facies core and granulite-facies rim, so eclogites must be older than ~21 Ma (Corrie et al. 2010). Accessory mineral ages of 13–14 Ma date granulite-facies conditions and subsequent cooling (Cottle et al. 2009, Corrie et al. 2010). Proportioning the Lu-Hf garnet age between eclogite and granulite components on the basis of measured core versus rim Lu contents, and assuming a youngest possible granulite-facies age of 13–14 Ma, implies a maximum age of eclogitization of 23–26 Ma (Corrie et al. 2010)—quite clearly younger than UHP eclogites in the northwestern Himalaya, which had already cooled through fission track closure by ~25 Ma (Schlup et al. 2003, Wilke et al. 2012).

SYNTAXES

Like the UHP eclogites, the syntaxes represent geographically restricted occurrences of unusually high-grade metamorphic rocks. The Nanga Parbat–Haramosh massif occupies the core of the Nanga Parbat syntaxis in the northwest Himalaya and exposes relatively high-P rocks along its eastern edge, including granulites, Ky + Kfs gneisses, and the Stak eclogite discussed above (e.g., Misch 1949, Pognante et al. 1993, Le Fort et al. 1997). Unusually young (≤3 Ma) leucogranites and low-P Crd + Kfs + Sil ± Spl LHS gneisses in the core of the massif have inspired numerous studies (see summaries in Zeitler et al. 1993, 2001a). Unfortunately from the perspective of quantitative petrology, only a handful of garnet zoning profiles and mineral compositions have been published for massif core rocks, petrologic criteria were not applied in compositional selection (nearly all are described as rim analyses), and most P-T conditions are inconsistent with petrogenetic grids. Sparse data for central gneiss garnets (Winslow et al. 1995) demonstrate significant diffusional reequilibration of garnet compositions and qualitatively explain discrepancies between thermobarometry and petrogenetic grids, but also render nearly all thermobarometric and P-T path calculations suspect. Detailed investigations of high-grade central gneisses at Nanga Parbat by Whittington et al. (2000) provide the best-constrained P-T estimate. Key assemblages and textures include the formation of cordierite and spinel after Bt + Sil, and together with measured spinel compositions restrict P-T conditions to T ≥ 700°C at 5 kbar (**Figure 7**). Textures and compositions do not directly constrain the P-T history, but structural setting favors nearly isothermal exhumation, crossing the muscovite-dehydration-melting curve to produce leucogranites (e.g., Zeitler & Chamberlain 1991, Whittington 1996, Butler et al. 1997, Zeitler et al. 2001a, Koons et al. 2002).

Rocks commonly assigned to the GHS in the core of the Namche Barwa massif display unusually high metamorphic grade (granulites and Crd + Spl–bearing assemblages) and young ages from leucogranites and leucosomes (≤4 Ma; Liu & Zhong 1997, Burg et al. 1998, Ding et al. 2001, Booth et al. 2004). Peak P-T conditions are difficult to constrain because observed assemblages are stable over a wide region of P-T space, and extensive low-P, high-T overprinting complicates thermobarometry. Nonetheless, T ≥ 800°C at a maximum P of 11–15 kbar is consistent with most data (Liu & Zhong 1997, Ding & Zhong 1999, Booth et al. 2009, Guilmette et al. 2011) (**Figure 7**). Thermobarometry of overprinting cordierite assemblages and detailed pseudosection analysis of melanosomes indicate nearly isothermal exhumation at T ≈ 800°C (Liu & Zhong 1997, Ding & Zhong 1999, Guilmette et al. 2011), although some heating during exhumation is possible (Guilmette et al. 2011). Guilmette et al. (2011) inferred melt crystallization in restites at T ≈ 800°C and P ≈ 10 kbar, which agrees broadly with isopleths of Ti content of quartz rims that are interpreted to have crystallized from in situ melts (**Figure 7**).

Geochronology of central gneisses at Namche Barwa (Burg et al. 1998; Ding & Zhong 1999; Ding et al. 2001; Booth et al. 2004; Xu et al. 2010, 2012; Liu et al. 2011; Su et al. 2012) yields conflicting interpretations. Ages assigned to high-T processes (3–40 Ma) bracket ages assigned to initial cooling (11–18 Ma). Constraints on the former include U-Pb zircon ages of deformed leucogranites and leucosomes (3–14 Ma; Booth et al. 2004), bulk monazite separates (4–19 Ma; Liu et al. 2011), a garnet Sm-Nd age (16.0 ± 2.5 Ma; Burg et al. 1998), and U-Pb ages of zircon linked chemically or texturally to high temperature (11–24, 40 Ma; Ding et al. 2001, Xu et al. 2010). Initial cooling ages include hornblende $^{40}Ar/^{39}Ar$ (8–17 Ma; Ding & Zhong 1999, Ding et al. 2001), amphibolite-facies zircons (17–18 Ma; Xu et al. 2010, Su et al. 2012), and monazite with rims that crystallized from in situ partial melts (11, 19 Ma; Liu et al. 2011). One admittedly nonunique scenario is that high-P granulite-facies metamorphism persisted until 17 Ma (zircon, garnet ages), succeeded by exhumation, melt crystallization at ~11 Ma (zircon,

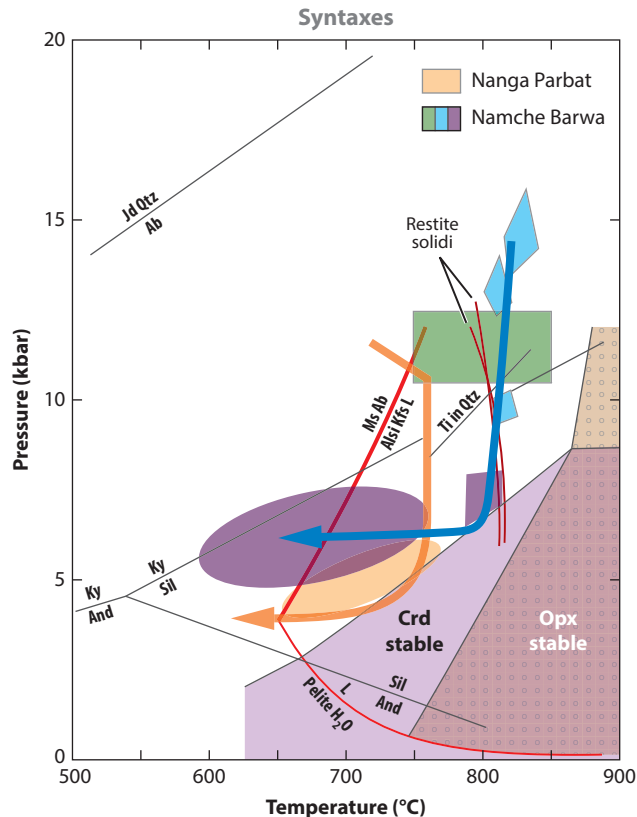**Kfs:** K-feldspar

Sil: sillimanite

Figure 7

P-T constraints for core massifs of the Nanga Parbat and Namche Barwa syntaxes. Boxes and ellipses represent specific P-T constraints (*orange ellipse*, Whittington et al. 2000; *purple fields*, Liu & Zhong 1997 and Ding & Zhong 1999; *green box*, recalculated data from Booth et al. 2009; *blue polygons*, Guilmette et al. 2011). Restite solidi are from Guilmette et al. (2011). Stability fields for cordierite and orthopyroxene are from Spear et al. (1999; see also **Figure 5**). Some published P-T fields are not included for petrologic reasons (e.g., see discussion in Burg et al. 1998, Guilmette et al. 2011). Abbreviations: Ab, albite; Alsi, aluminosilicate; And, andalusite; Crd, cordierite; Jd, jadeite; Kfs, K-feldspar; L, liquid; Ms, muscovite; Opx, orthopyroxene; Qtz, quartz; Sil, sillimanite.

monazite), and cooling through the amphibolite facies at ∼8 Ma (^{40}Ar/^{39}Ar ages), but with sporadic intrusion of leucogranites, local reheating, and mineralization as recently as 3 Ma (youngest leucogranites).

ACCESSORY MINERAL THERMOMETRY AND GEOCHRONOLOGY: THE PACE OF CHANGE

Advances in four key areas of accessory mineral geochemistry and geochronology are revolutionizing petrologic methods and beginning to shape our understanding of Himalayan tectonics: (*a*) experimental calibration of the strong temperature dependence of Zr contents in rutile and titanite and Ti contents in zircon and quartz (e.g., see Watson et al. 2006, Hayden et al. 2008, Thomas et al. 2010); (*b*) petrologic and geochemical models of abundances (dissolution versus growth) and chemical variations in monazite and zircon (Rubatto 2002, Kelsey et al. 2008, Spear

& Pyle 2010, Kelsey & Powell 2011); (*c*) rapid and precise microanalysis, particularly by LA-ICP-MS (laser-ablation, inductively coupled plasma mass spectrometry); and (*d*) X-ray mapping or other imaging of genetically distinct chemical domains. Combining geochemistry, petrology, and geochronology now constrains Ts much more precisely and, in favorable cases, links accessory mineral ages with the P-T conditions of formation. Three examples illustrate the potential of these methods but also raise new petrologic and tectonic questions.

Monazite

In most rocks, a single trace element cannot as yet link monazite chemistry directly to T. Rather, Y and Th zoning patterns, as identified using X-ray mapping, are combined with petrogenetic considerations and other trace element patterns to allow inference of the reactions responsible for producing earlier- versus later-formed Mnz (see Pyle & Spear 1999, 2003; Zhu & O'Nions 1999; Kohn et al. 2005). For example, prograde growth of garnet and monazite sequesters Y and Th, so that later-formed grains or domains have lower Y and Th contents. Thus, in lower-grade GHS and LHS, latest-formed domains or grains can be identified chemically and dated microanalytically to estimate the peak metamorphic age. Monazite dissolves during melting (Kelsey et al. 2008, Spear & Pyle 2010) and regrows with a high Y and Th content when the melt cools and crystallizes (Pyle & Spear 2003). Thus, in migmatitic GHS, monazite typically exhibits high-Y and high-Th rims (melt crystallization) that overgrow preanatectic low-Y cores (Kohn et al. 2004, 2005) (**Figure 8a**). Geochronology of monazite domains in migmatites principally dates the timing of melt crystallization (monazite rim ages) and brackets the timing of peak metamorphism and melting (monazite rim versus core ages).

Data from central Nepal (Kohn et al. 2004, Corrie & Kohn 2011) illustrate two major features (**Figure 8a**; see also Montomoli et al. 2013 for analogous data from western Nepal). First, the age of each generation of monazite decreases structurally downward—e.g., along the Modi transect, late prograde ages decrease from ca. 35 to <25 Ma, whereas at Langtang peak, metamorphic ages decrease from ca. 20 and 16 Ma in the middle and lower GHS to 11 and 3 Ma in the upper and lower LHS, respectively (**Figure 8a**). Second, cooling at higher structural levels coincides with heating at lower structural levels—at Langtang, rocks of the lower GHS were still heating while melts in the middle GHS were crystallizing, rocks of the upper LHS were still heating while melts in the lower GHS were crystallizing, etc. These patterns are expected for in-sequence thrusting because thrust emplacement cools the hanging wall while heating the footwall. Thus, in central Nepal, the upper GHS was transported soon after 25 Ma, the MCT was active between ca. 15 and 20 Ma, and LHS thrusts were active later. Note that older ages approaching 40 Ma say little about metamorphic conditions because monazite can form at temperatures ranging from diagenesis (e.g., Evans & Zalasiewicz 1996) to melt crystallization.

Titanite

Few studies as yet analyze titanite, but combination of in situ Zr-in-Ttn thermometry with U-Pb geochronology in central Nepal constrains T-t histories for high-grade GHS (Kohn & Corrie 2011) (**Figure 8b**). Titanite crystals from calc-silicates along the Modi transect (**Figures 1** and **3b**) were analyzed using LA-ICP-MS for Zr content and U-Pb ages, both in thin section with simple spot analyses and as mineral separates via depth profiling. These data appear unaffected by diffusional reequilibration of either Zr or Pb and indicate T ≥ 700–750°C since ~35 Ma, peaking at T ≈ 775°C at ~20 Ma (**Figure 8b**). This latter result compares well with monazite rim ages from the same region that indicate melt crystallization at ~19 Ma (**Figure 8a**). However, monazite

core ages of 25–35 Ma are interpreted to reflect subsolidus conditions, whereas Zr-in-Ttn Ts are above expected pelite solidi (Spear et al. 1999). Either (*a*) unrecognized bias affects Zr-in-Ttn Ts or ages, (*b*) monazite petrogenesis of core compositions is misinterpreted (e.g., low-Y cores reflect dissolution-reprecipitation in the presence of melt, not prograde subsolidus growth), or (*c*) the solidi of metapelites are higher than predicted thermodynamically. Regarding the latter, some experiments (Patiño Douce & Harris 1998) suggest solidus Ts 25–50°C higher than the solidus predicted by petrogenetic grids and pseudosections (e.g., Spear et al. 1999, Guilmette et al. 2011, Groppo et al. 2012). Thermobarometric and Zrc-saturation Ts, however, are consistently lower than in the Patiño Douce & Harris experiments (**Figures 4** and **8c**).

Zrc: zircon
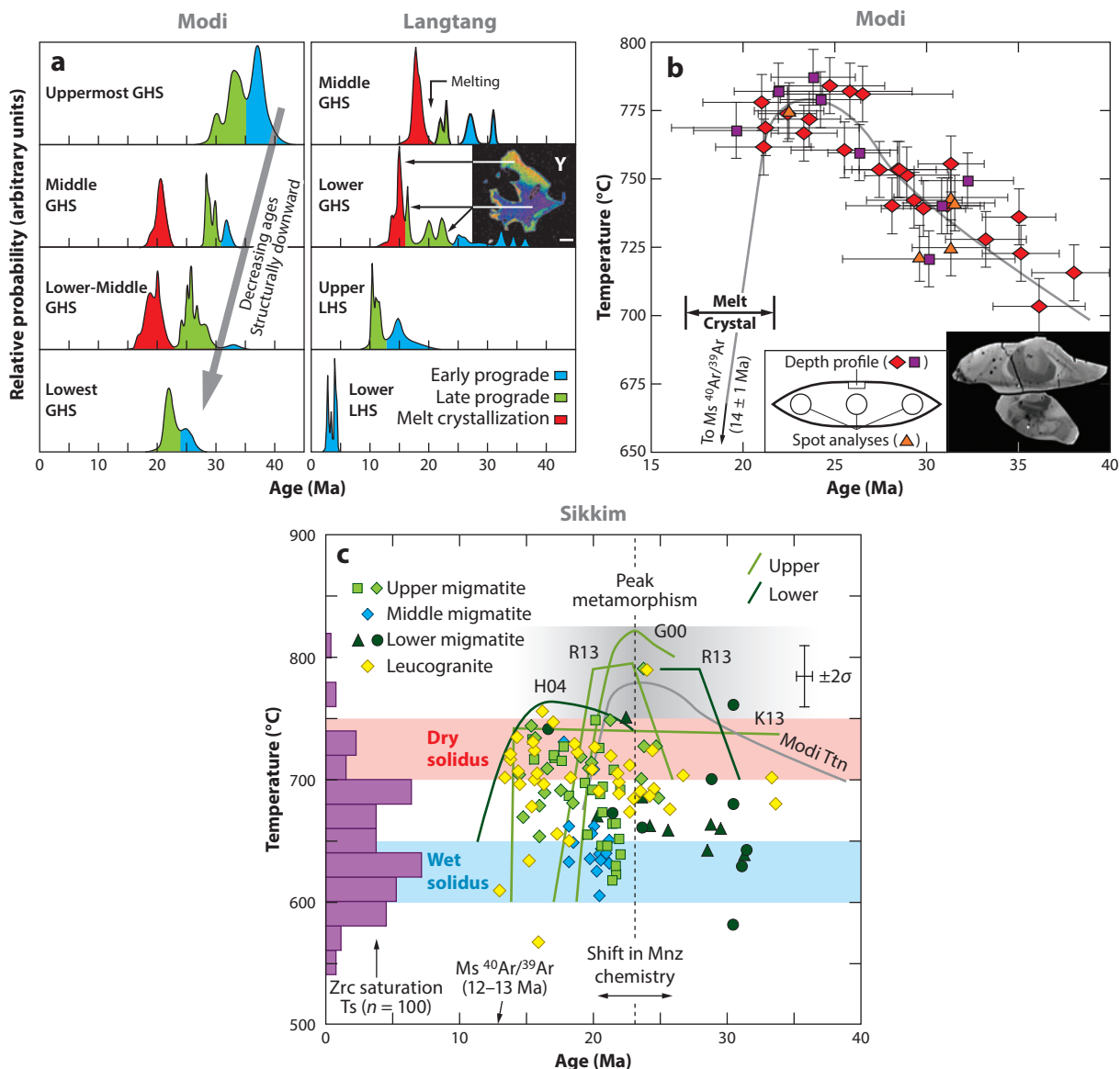
Zircon

Novel combination of Ti-in-Zrc thermometry and U-Pb geochronology is most comprehensive for leucogranites and migmatites from high-grade GHS of Sikkim (Kellett et al. 2013, Rubatto et al. 2013). Muscovite dehydration melting is thought to have produced partial melts in migmatites and discrete leucogranite bodies (Inger & Harris 1992, Harris & Massey 1994), in principle allowing intercomparison of these two data sets. Ti-in-Zrc Ts depend on the activity of rutile [a(Rt)], and Ts were recalculated from reported Zr concentrations assuming average metapelite a(Rt) = 0.8 ± 0.2 (Chambers & Kohn 2012); in fact, a(Rt) was likely higher (calculated Ts are maxima) because rutile is reported in some rocks, and biotite compositions (Neogi et al. 1998, Dasgupta et al. 2004, Harris et al. 2004, Rubatto et al. 2013) imply a(Rt) > 0.95 at estimated peak Ts of 750–825°C. Decreasing a(Rt) to 0.5 increases Ti-in-Zrc Ts by ~50°C. The Zr content of melts in equilibrium with zircon is also temperature sensitive (Watson & Harrison 1983), and the latest experimental calibration (Boehnke et al. 2013) was used to estimate typical leucogranite melt Ts for tabulated compositions from the central Himalaya (see references in the **Supplemental Material**). Use of the Watson & Harrison (1983) calibration raises Zrc-saturation Ts by ~50°C. Ti-in-Zrc Ts broadly range between wet and dry solidi and overlap Zrc-saturation Ts (**Figure 8c**). Migmatites may suggest gradually increasing T to ~16 Ma, although chemistry of monazite and zircon suggests peak Ts at 23–28 Ma (depending on structural level) and a transition to initial cooling at 20–25 Ma (Kellett et al. 2013, Rubatto et al. 2013) (**Figure 8c**).

In the context of published T-t paths (**Figure 8c**), zircon Ts are perplexing. First, no zircon should record a T below the T-t path, yet they consistently do. How can a 650°C zircon crystallize in an 800°C rock? Second, if regional Ts were low when the first zircon crystallized in leucosomes or leucogranites, but Ts increased through time, then the leucosomes and leucogranites should remelt, dissolving older zircons. So, why are older zircons preserved? More generally, many studies for the area invoke heating followed by high-T exhumation to catalyze melting between 25 and 15 Ma (e.g., Ganguly et al. 2000, Harris et al. 2004, Groppo et al. 2012, Kellett et al. 2013, Rubatto et al. 2013), yet progressive melting should cause zircon to dissolve, not crystallize (Kelsey et al. 2008, Kelsey & Powell 2011). Several possible explanations can be considered but are as yet unsatisfying: (*a*) Calculated Ti-in-Zrc Ts are too low. Experimental and natural data are mutually consistent (Watson et al. 2006), however, and a(Rt) would have to be unreasonably low (~0.25) to raise calculated Ts to ~800°C. (*b*) Estimated regional metamorphic Ts are too high. Petrogenetic

Rt: rutile

▶ Supplemental Material

Figure 8

Geochronologic constraints from the central Himalaya that directly link to T histories. (*a*) Monazite chemistry can be linked to progressively higher grades (decreasing Y and Th) and crystallization of in situ melts (high-Y, high-Th rims). Ages from central Nepal show systematically decreasing ages structurally downward for each monazite generation, consistent with in-sequence thrusting (Kohn et al. 2004, Corrie & Kohn 2011; modified with permission from Elsevier). Inset shows an X-ray map of yttrium (Y) that illustrates pre- versus postanatectic monazite generations in a single grain. (*b*) Titanite Ts (from Zr-in-Ttn thermometry) and U-Pb ages indicate increasing Ts from 35–40 Ma to ~20 Ma (Kohn & Corrie 2011; modified with permission from Elsevier). Insets show backscattered electron image of titanite, illustrating complex zoning and multiple generations of titanite, and analytical protocol (either spot analysis in polished thin sections or depth profiling of separated grains). "Melt crystal" refers to regional ages for melt crystallization as determined from monazite. (*c*) Zircon T-t data from in situ Ti-in-Zrc and U-Pb (Kellett et al. 2013, Rubatto et al. 2013), shaded according to structural level. Data suggest T ≤ ~700°C since 35 Ma, and possibly increasing Ts to ~15 Ma. Ti-in-Zrc and typical Himalayan Zrc-saturation Ts (histogram on left; see **Supplemental Material** for references) fall well below estimated peak metamorphic Ts. A shift in monazite chemistry at 20–25 Ma may indicate a transition to regional cooling. The gray curve reproduces the Modi titanite-derived T-t history. Other T-t curves are from Ganguly et al. (2000; G00, assuming peak age of 23 Ma), Harris et al. (2004; H04), Rubatto et al. (2013; R13), and Kellett et al. (2013), and are shaded according to structural level. Geologic abbreviations: GHS, Greater Himalayan Sequence; LHS, Lesser Himalayan Sequence. Mineralogic abbreviations: Mnz, monazite; Ms, muscovite; Ttn, titanite; Zrc, zircon.

grids and pseudosections consistently require T ≈ 800°C to explain occurrences of cordierite and spinel in metapelites (Spear et al. 1999, Ganguly et al. 2000, Groppo et al. 2012, Rubatto et al. 2013) and orthopyroxene in metabasites (Neogi et al. 1998, Pattison et al. 2003). Otherwise, if petrologic Ts are not regional, then every occurrence of high-grade assemblages would have to reflect an anomaly near an intrusion. (*c*) The ages are incorrect. The systematic correlation of zircon chemistry and ages (see Rubatto et al. 2013) and general reliability of zircon U-Pb ages make this unlikely. (*d*) The age of peak metamorphism and low-P assemblages predates granite and migmatite crystallization. This would generally require peak metamorphism at ≥35 Ma, which is inconsistent with mineral chemical trends (Rubatto et al. 2013) and regional chronologic patterns (e.g., Godin et al. 2006).

TECTONIC MODELS

Tectonic models of Himalayan metamorphism have mainly focused on four questions: How did an inverted metamorphic field gradient form across the MCT? To what degree does flow of middle to lower crust (channel flow) impact metamorphic evolution? What mechanism drove extension? How and why were eclogites and granulites exhumed? Answers to these questions can generally be divided into either continuum processes or singular events. Thermal models (e.g., channel flow, critical wedge) typically represent continuum responses to specific boundary conditions. Singular events include specific shear zone movements, wedge collapse, slab breakoff, and structural or erosional focusing at the syntaxes.

Several models emphasize links among climate, erosion, tectonics, and metamorphism (e.g., see Willett 1999, Beaumont et al. 2001, Koons et al. 2002). Regionally, modern precipitation in the Himalaya varies from a high of 2,000–4,000 mm/yr in the frontal portion of the range to as little as 100 mm/yr toward the hinterland (e.g., Bookhagen & Burbank 2006). Modern erosion rates at the range front can exceed 5 mm/yr (Lavé & Avouac 2001), although longer-term rates are generally lower and do not obviously correlate with rainfall (Burbank et al. 2003, Thiede et al. 2009). Local erosion rates ≥5 mm/yr occur along specific rivers such as the Indus (Nanga Parbat syntaxis; Zeitler et al. 2001b) and Yarlung Tsangpo (Namche Barwa syntaxis; Burg et al. 1998), especially where they cross the range.

Origin of Inverted Metamorphism

Originally Le Fort (1975) proposed that rapid emplacement of the GHS along the MCT and downward heat conduction into the LHS produced the metamorphic inversion. Viability of this singular event model also requires significant shear heating and rapid exposure to prevent thermal equilibration of the footwall (England & Molnar 1993b). Others proposed postmetamorphic

---

Figure 9

Models of orogenic wedges and the development of the inverted metamorphic gradient. (*a*) Conceptual model of extrusion (Grujic et al. 1996; modified with permission from Elsevier) overturns isograds (*dashed and dotted lines*) along the lower thrust boundary. (*b*) Channel flow thermal model (modified from Jamieson et al. 2004). Focused erosion at the orogenic front (*large gray arrow*) couples with hot, partially molten GHS. Stippling shows the region fertile to melting. Shear zones are not proscribed, so MHT and STDS locations are based on strain gradients. The length of long versus short white arrows below and above the MHT is proportional to the magnitude of shear along the MHT versus channel flow. (*c*) Relatively cold critical wedge model (modified from Henry et al. 1997, Cattin & Avouac 2000, Kohn 2008) with distributed erosion (*small gray arrows*). Black squares show the P-T positions of different thrust sheets at Langtang. Geologic abbreviations: GHS, Greater Himalayan Sequence; LHS, Lesser Himalayan Sequence; MHT, Main Himalayan Thrust; STDS, South Tibetan Detachment System; THS, Tethyan Himalayan Sequence. Mineralogic abbreviations: Ab, albite; Alsi, aluminosilicate; And, andalusite; Kfs, K-feldspar; Ky, kyanite; L, liquid; Ms, muscovite; Qtz, quartz; Sil, sillimanite.

folding of isograds (e.g., Searle & Rex 1989, Hubbard 1996) and postmetamorphic shearing, in the context of either thrust-sense shearing at multiple levels (Jain & Manickavasagam 1993) or extrusion bounded by thrust- and normal-sense shears (Grujic et al. 1996, Vannay & Grasemann 2001) (**Figure 9a**). Fold nappes at scales of several kilometers do occur in northwestern India (Searle & Rex 1989), but they do not postdate peak metamorphism there (Wyss 2000, Walker

POSTMETAMORPHIC EXTRUSION
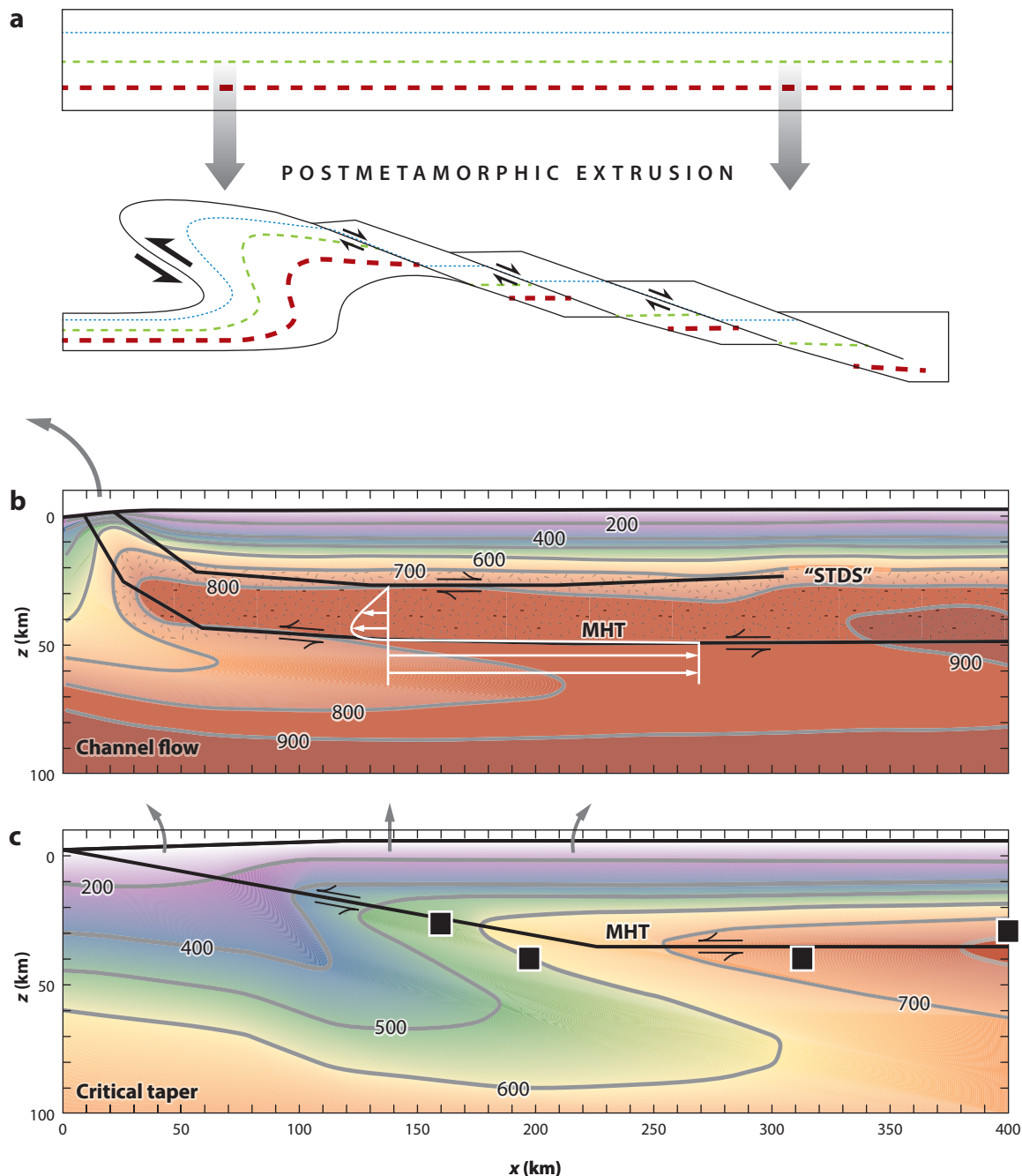
et al. 2001), and such folds are not generally evident elsewhere. More relevantly, many of these models implicitly presume a normal geotherm (i.e., Ts increase downward uniformly) with flat isotherms and isograds (**Figure 9a**), so that juxtaposition of higher-grade on lower-grade rocks reflects an anomalous perturbation to an otherwise monotonous thermal structure. Each model ignores one of two basic facts. First, just because a thrust slice reached high temperatures does not mean it was emplaced hot—it might have cooled during or prior to emplacement so that isotherms during emplacement were not significantly perturbed from steady state. Second, just as in subduction zones, most models of protracted continental underthrusting produce sigmoidal, not flat, steady-state isotherms (Royden 1993, Henry et al. 1997) (**Figure 9b,c**). That is, at scales of tens of kilometers, isotherms of the middle to lower crust are inherently folded even if the rocks are not. In principle, lateral transport alone through such a thermal structure could produce an inverted metamorphic gradient or metamorphic sandwich (Kohn 2008) without requiring folding or differential extrusion of the Himalayan core.

Ultimately, chronologic microanalysis of monazite solved the inverted metamorphism problem, at least in central Nepal, in favor of simple lateral transport via a continuum of in-sequence thrusts. First, Grt-grade (~550°C) LHS rocks immediately beneath the MCT in central Nepal exhibit considerably younger prograde to peak metamorphic ages (6–8 Ma) than those of the overlying GHS (≥20 Ma; Harrison et al. 1997, Catlos et al. 2001). Notably, the LHS ages are younger than GHS muscovite ^{40}Ar/^{39}Ar ages (10–20 Ma depending on structural level; e.g., see Herman et al. 2010), which presumably record cooling through ~425°C (Harrison et al. 2009). So the GHS was undoubtedly cooler than the LHS when the LHS was metamorphosed, and the geotherm in the middle to upper crust was not inverted at that time or location. Second, Kohn et al. (2004) documented simultaneous cooling of hanging wall rocks during heating of footwall rocks across three major in-sequence thrusts in the Langtang region (**Figure 8a**; see also Carosi et al. 2010, Corrie & Kohn 2011, Montomoli et al. 2013). These results imply greater dynamism between structure and metamorphism but are nonetheless expected for steady-state models of protracted thrusting. Singular structural and thermal perturbations could have occurred, such as postmetamorphic folding or shearing, but general metamorphic and chronologic observations do not require them.

Protracted in-sequence thrusting helps explain several major structural and metamorphic features (Kohn 2008). For example, reconstruction of sample paleopositions in the context of steady-state thermal models suggests that each major in-sequence thrust, when active, was simply the shallowly inclined MHT (**Figure 9c**). As the MHT stepped downward in response to changes in wedge thickness or geometry, its former abandoned trace was passively carried forward and eventually exhumed. We now label these former traces as separate thrusts because they juxtapose different rock types, but when active they were simply the MHT (obviously this does not apply to out-of-sequence thrusts). In-sequence thrusting further implies that metamorphic gradients broadly reflect the scale and duration of thrusting. Long transport on a single shear zone juxtaposes rocks of considerably different metamorphic grade to produce steep metamorphic gradients. In contrast, short transport juxtaposes rocks of similar metamorphic grade, and accumulation of numerous such thrusts in a duplex produces shallow metamorphic gradients. Presumably this is why the MCT and LHD exhibit such different P and T gradients (**Figure 4**): They respectively reflect long transport on a single thrust (steep gradient on the MCT) and accumulation of numerous short-transport thrusts (shallow gradient on the LHD).

Orogenic Channels: Flow or No Flow?

Numerous thermal-mechanical simulations have resolved into a dichotomy of orogenic wedge models—normally termed channel flow and critical taper—to explain the distribution of

LHS-GHS-THS metamorphic rocks (**Figure 9*b,c***). In channel flow (Beaumont et al. 2001, Jamieson et al. 2004) (**Figure 9*b***), weak, partially molten material in the mid- to deep crust (nominally the GHS) couples with and flows toward a focused erosional front, differentially transporting heat and mass relative to stiffer rocks above and below (nominally the THS and LHS). Basically, if erosion differentially removes material at the range front, the channel flows forward to replace that material, with greater flow at the base of the channel where rocks are weakest. In critical taper models (e.g., Dahlen 1990) (**Figure 9*c***), erosion is distributed and the wedge maintains a regular, material-specific geometry without requiring lower crustal flow, typically deforming through in-sequence thrusting. Focused erosion, if it occurs, is balanced proximally through the development of a thrust duplex (Dahlen 1990, Herman et al. 2010), and extension reflects a singular adjustment to wedge mechanical properties such as rheology or basal shear stress. Whereas the channel flow model of metamorphic and chronologic evolution can ultimately be traced to a particular thermal-mechanical simulation (Beaumont et al. 2001), models referred to as critical taper include mechanical-only models (Dahlen 1990), steady-state thermal models (Henry et al. 1997), and thermal models with evolving kinematics (Herman et al. 2010). These latter models differ in approach but, like critical taper sensu stricto, exhibit consistent wedge geometries and boundary conditions.

Few question whether GHS rocks weakened thermally and through in situ partial melting. Whether a sufficient thickness of crust was simultaneously weak and actually did flow, however, has sourced intense debate for over a decade. Reserving quantitative P-T-t considerations for later discussion, arguments in favor of channel flow include the following: (*a*) Focused erosion at the range front can catalyze flow, and this erosional pattern is observed today. (*b*) Flow of a channel explains the STDS. All orogenic models include thrusting along the base of the wedge, but channel flow additionally implies long-term (tens of millions of years) normal-sense shear along the channel top. (*c*) Channel flow produces a metamorphic sandwich. Differential extrusion of a high-T central channel amplifies metamorphic gradients both above and below.

Arguments in favor of critical taper include the following: (*a*) Focused erosion can catalyze duplex formation (Dahlen 1990, Herman et al. 2010), and a duplex is observed (the LHD). (*b*) The duration of movement on the STDS in some areas may have been only a few million years (Sachan et al. 2010, Carosi et al. 2013), which points to short-lived adjustment to wedge geometry. The STDS may not even have formed in northwestern India, despite broad metamorphic and structural similarities to other regions along strike. (*c*) Most continuum models, including critical taper, form a metamorphic sandwich (e.g., Royden 1993, Henry et al. 1997, Cattin & Avouac 2000, Herman et al. 2010). (*d*) Juxtaposition of rocks with differing metamorphic grades should occur at depth along the décollement (MHT), not a thrust ramp. Structural studies consistently demonstrate emplacement of the main thrust sheets with a flat-on-flat, not inclined, geometry (Robinson & Pearson 2006) (**Figure 1*c–e***).

Of relevance to this review, these two end-member models make distinctly different P-T-t predictions (Kohn 2008) (**Figure 10**). Channel flow's high heat production and profound lateral heat transport increase Ts of over- and underlying rocks by ~150°C nearly isobarically (**Figure 10*a***). Most heat transport in these models actually occurs via thrust displacement, rather than flow sensu stricto: Model particle paths suggest ~80 km of transport from flow (Jamieson et al. 2004) (**Figure 9*b***), versus minimum thrust displacements of 500–900 km (see summary in Long et al. 2011). In contrast, critical taper's in-sequence thrusting rapidly loads rocks beneath the MHT, then soon after exhumes them as the MHT steps to a lower level, so the prograde path remains in the kyanite stability field (**Figure 10*b***). Very generally, channel flow predicts (**Figure 10*a,c***) (*a*) high-T, low-P metamorphic arrays in the andalusite and sillimanite stability fields, (*b*) isobaric heating P-T paths for LHS and THS and isothermal exhumation paths for GHS, and (*c*) nearly synchronous initial cooling of all metamorphic levels, especially linking
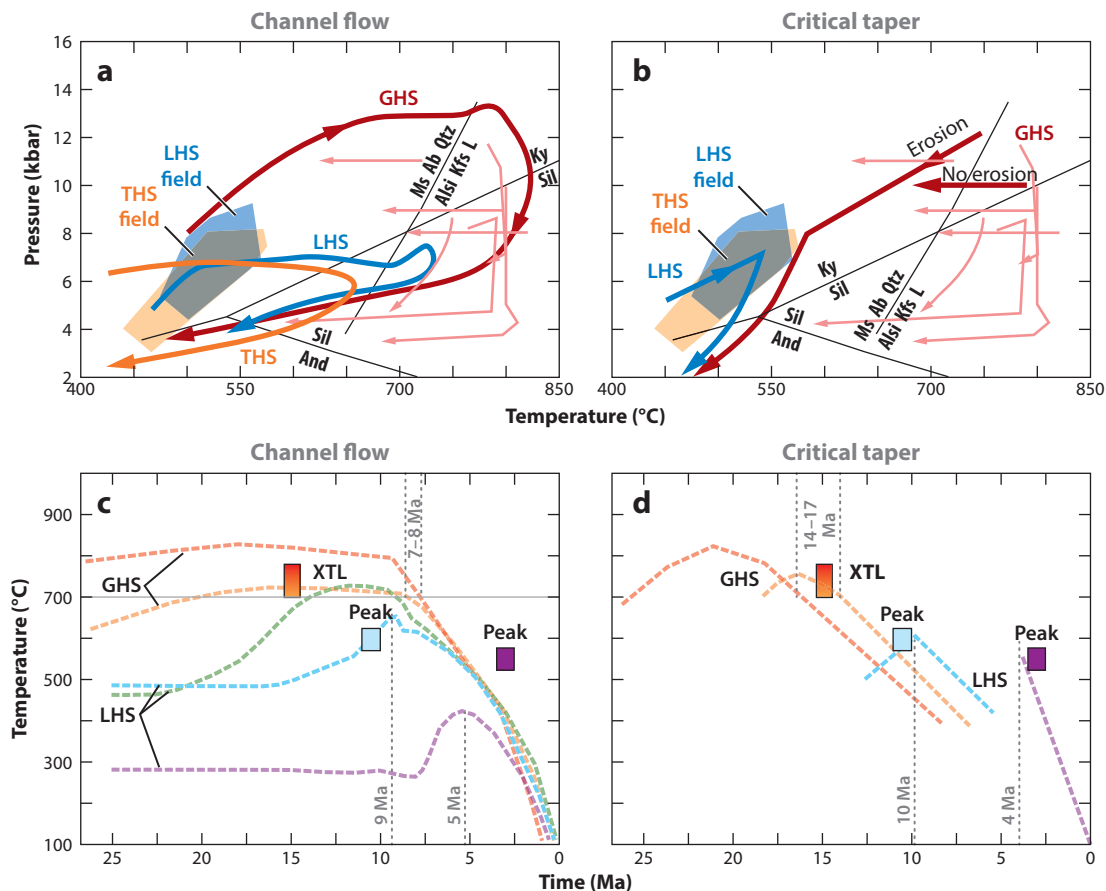
Figure 10

Wedge model–predicted P-T paths in comparison with data. (*a,b*) Predicted P-T paths (*heavy arrowed lines*), reported GHS P-T paths (*thin pink lines*) (Ganguly et al. 2000, Harris et al. 2004, Kohn 2008, Groppo et al. 2012, Rubatto et al. 2013), and region of LHS and THS P-T paths (*blue and orange fields*) (see **Figure 5c**). (*c,d*) Predicted T-t paths (*colored dashed lines*) and petrologically significant times (*gray dotted lines*) in comparison with data from Langtang (*squares*) (Kohn 2008). Model paths are based on Jamieson et al. (2004), Kohn (2008), Herman et al. (2010). Geologic abbreviations: GHS, Greater Himalayan Sequence; LHS, Lesser Himalayan Sequence; THS, Tethyan Himalayan Sequence. Mineralogic abbreviations: Ab, albite; Alsi, aluminosilicate; And, andalusite; Kfs, K-feldspar; Ky, kyanite; L, liquid; Ms, muscovite; Sil, sillimanite. Other abbreviations: Peak, peak metamorphic age (bracketed by lowest-Y Mnz cores and high-Y Mnz rims); XTL, crystallization of in situ melts (growth of high-Y Mnz rims at ~700°C).

crystallization of in situ melts in the GHS hanging wall with peak metamorphism in the LHS footwall. In contrast, critical taper predicts (**Figure 10b,d**) (*a*) intermediate P-T arrays in the kyanite stability field, (*b*) limited heating P-T paths for LHS and THS, and (*c*) systematically decreasing metamorphic ages structurally downward. Critical taper's predicted P-T paths for GHS rocks depend on specific models, which include isobaric cooling (Kohn 2008), exhumation with cooling (Herman et al. 2010), and isothermal exhumation (Huerta et al. 1999).

Many petrologic and chronologic observations are more consistent with critical taper (Kohn 2008) (**Figure 10b,d**), including relatively cool P-T conditions within the kyanite stability field (**Figure 4**), LHS and THS P-T paths that show limited heating (**Figure 5**), some GHS P-T paths that show isobaric cooling (**Figure 10b**), and T-t histories that demonstrate significant decreases

in metamorphic ages structurally downward with a significant time lag between melt crystallization in the hanging wall and peak metamorphism of the footwall (**Figure 10b**). Some observations are consistent with both models, particularly the large temperature gradient in the region of the MCT (**Figure 4**). GHS P-T paths involving high-T isothermal exhumation (**Figure 5**) are generally more consistent with channel flow (**Figure 10b**) because qualitatively similar paths are intrinsic to channel flow but to only a subset of critical taper models.

Whereas low-P, high-T overprinting assemblages and repeated intrusion of leucogranites, particularly from Nyalam through western Bhutan, are commonly linked to channel flow (e.g., Davidson et al. 1997), they do carry petrologic ambiguities. First, incompatibilities between regional metamorphic Ts and leucosome and leucogranite Ti-in-Zrc and Zrc-saturation Ts (**Figure 8c**) raise questions about the genetic links between leucogranites and regional metamorphism. Repeated crystallization of relatively low-T melts would seem to imply cold country rocks, arguably <~300°C since ~20 Ma in the Everest region (Viskupic et al. 2005). Second, channel flow–induced decompression melting to form leucosomes and leucogranites should produce one major pulse of melting, rather than the protracted repeated intrusion that is commonly observed (Harrison et al. 1999) (**Figure 8c**). Last, Pognante & Benna (1993) hypothesized that low-P, high-T assemblages do not reflect a single exhumational continuum but rather overprinting thermal pulses (polymetamorphism; see also Visona et al. 2012). Yet, what could source such heat? Leucogranite intrusions several kilometers thick (e.g., Searle 1999) could locally heat surrounding rocks, but most leucogranites are probably not sufficiently large, hot, widespread, or synchronous to affect such a large sector. Increased mantle heat flux (e.g., from asthenospheric upwelling in the wake of slab breakoff; Kohn & Parkinson 2002), high radioactive heat production (Rao et al. 1976), and heat refraction below the THS (low thermal conductivity in THS rocks; Pinet & Jaupart 1987) could all fuel anomalously high Ts, possibly generating some leucogranites (e.g., Guilmette et al. 2011, Groppo et al. 2012). But these processes operate on long timescales (tens of millions of years), and it is unclear how they would cause thermal overprinting only ~10 Myr after maximum Ps were reached (e.g., see data in Corrie et al. 2010, Rubatto et al. 2013).

Models of Extension

Common models for the formation of the STDS and its impact on metamorphism include wedge collapse, channel flow, and wedge insertion. Wedge collapse assumes that high topography or changing physical properties trigger a singular flattening event (e.g., Burchfiel & Royden 1985, England & Molnar 1993a) (**Figure 11a**), which can homogeneously flatten the forward portion of a wedge while the rear of the wedge undergoes heterogeneous extension, forming the STDS (**Figure 11a**). Channel flow (Beaumont et al. 2001, Jamieson et al. 2004) (**Figure 11b**) requires long-term normal-sense shear along the channel's upper boundary to permit forward flow of the weak channel. In wedge insertion (passive roof thrust or tectonic wedging; e.g., Yin 2006), the STDS forms as the GHS is inserted between the THS and LHS (**Figure 11c**).

All these models can explain an upward continuous or discontinuous decrease in T from the GHS to the THS depending on mode of deformation and magnitude of shear, but they make different predictions about P distributions (**Figure 11**). Sparse data from northwestern India (**Figure 4b**) suggest a lithostatic gradient, perhaps indicating an absence of the STDS there (**Figure 3a**). Otherwise, a THS outlier in the Shemgang region of central Bhutan (**Figures 1**, **3c**, and **4k**) provides the most comprehensive data set (Corrie et al. 2012). These rocks occupy the frontal portion of GHS and THS exposures and exhibit a linear P distribution that is ~2 times steeper than lithostatic. This gradient indicates that the entire section has been homogeneously thinned or flattened by a factor of ~2 (from ~20 to ~10 km thickness), consistent with wedge
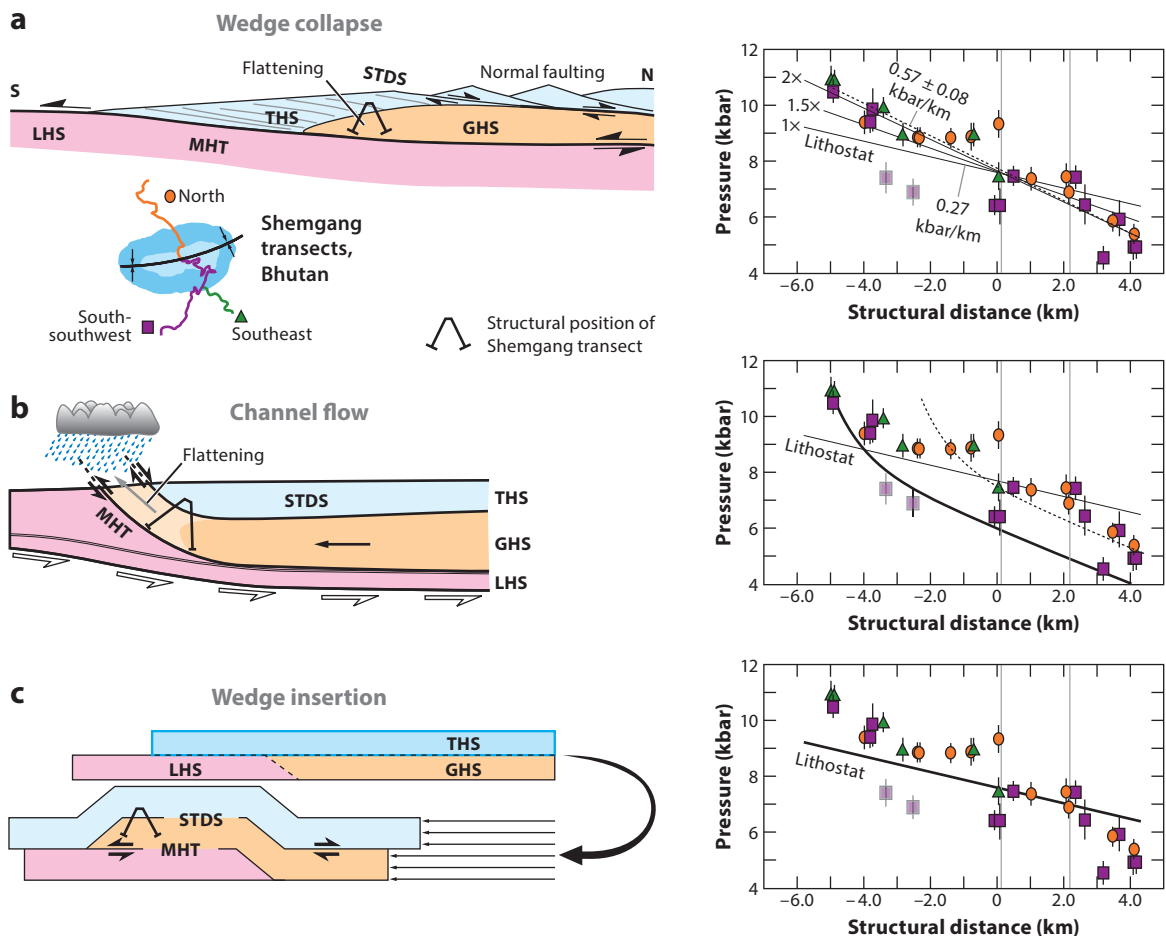
Figure 11

Models of development of the STDS and implications for the distribution of P versus structural distance in comparison with data from THS outlier in the Shemgang region, central Bhutan (**Figures 1** and **3c**) (*a*) Wedge collapse (Corrie et al. 2012; modified with permission from Elsevier): homogeneous flattening toward the foreland and extensional faulting (STDS) toward the hinterland. The magnitude of flattening defines P versus structural distance: No flattening (1×) yields lithostatic gradient, and increased flattening (1.5×, 2×) yields increasingly steep (superlithostatic) gradients. The observed gradient implies ∼2× flattening. The inset shows distributions of transects across the THS synclinal outlier. (*b*) Channel flow (modified from Godin et al. 2006): postmetamorphic flattening in the channel orifice. The black curve of P versus distance is based on Jamieson et al. (2004). The dashed curve shows the best fit to data but implies a different structural relationship to the MCT. (*c*) Wedge insertion (modified from Yin 2006): no flattening predicted. Abbreviations: GHS, Greater Himalayan Sequence; LHS, Lesser Himalayan Sequence; MHT, Main Himalayan Thrust; STDS, South Tibetan Detachment System; THS, Tethyan Himalayan Sequence.

collapse (**Figure 11a**). Channel flow also predicts postmetamorphic flattening, but the observed P gradient should increase with decreasing structural level because deeper, hotter, and weaker rocks should be flattened more (**Figure 11b**). Changing the T and rheological distributions might reconcile models and observations but might also shut down flow. Current wedge insertion models do not include flattening (**Figure 11c**), but it is also not precluded. Superlithostatic P gradients also occur at Langtang and Kumaun (**Figure 4e**) and may point to flattening as a common process.

Exhumation of Eclogites and Granulites

UHP eclogites must form in all subduction zones, but they rarely appear on Earth's surface. In the Himalaya, peak pressures for exposed UHP rocks were reached 5–10 Myr after the initiation of collision. Why were these particular UHP rocks exhumed, and no others (that we know of)? Classically, slab breakoff has been favored, in which the leading edge of the continental slab first is dragged to UHP depths by dense oceanic lithosphere, then rebounds buoyantly as the oceanic slab detaches (e.g., Chemenda et al. 2000, Kohn & Parkinson 2002) (**Figure 12a**). A thrust slice of upper crustal UHP rocks is rapidly emplaced at high structural levels, where it undergoes slower exhumation and cooling. Although this scenario is perhaps qualitatively plausible, comprehensive numerical analysis (Warren et al. 2008a,b) demonstrates that upper crust can simply detach from the denser lower crust and lithospheric mantle without slab breakoff. Instead, corner flow develops in the early stages of continental subduction, rapidly returning a slab of continental UHP rocks to the middle crust (**Figure 12b**). Alternatively, a transition from subduction of thinned weaker
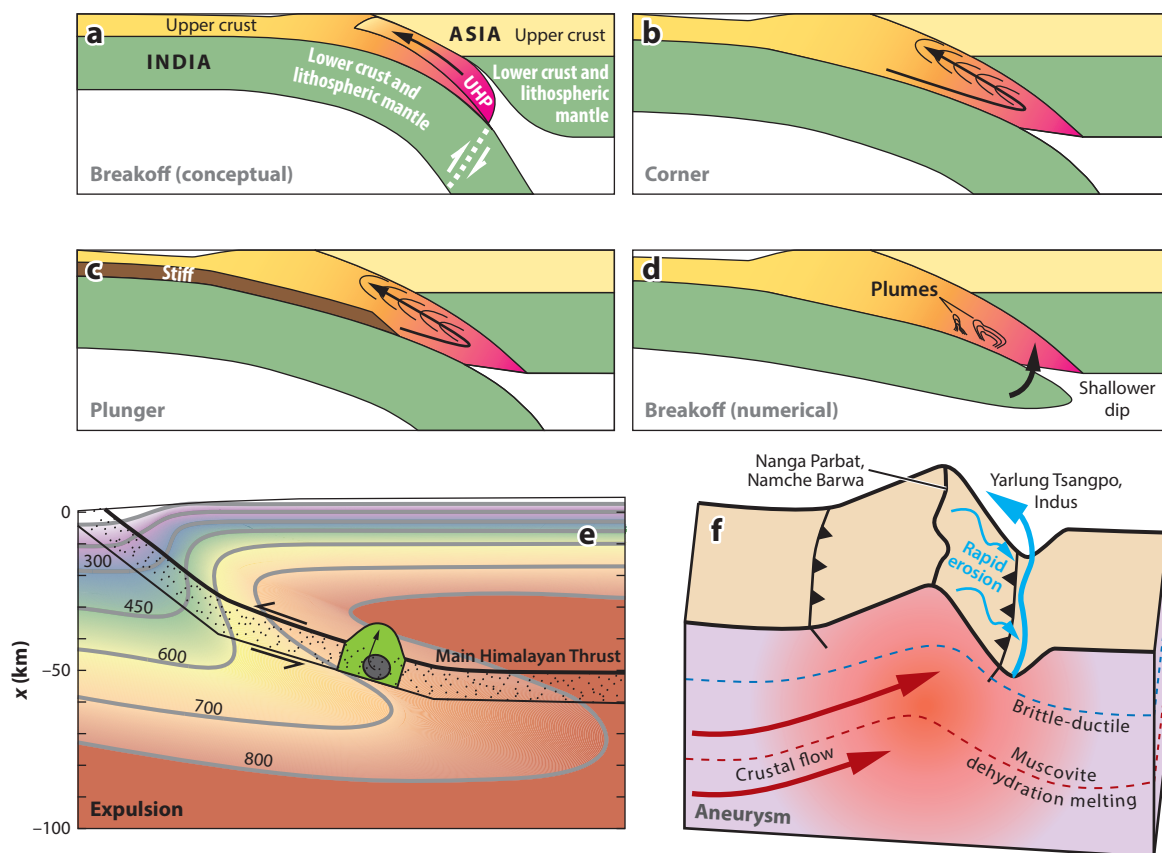

Figure 12

Models of exhumation of eclogites and granulites. (*a*) Conceptual model (Chemenda et al. 2000) and (*b–d*) numerical models (Warren et al. 2008a,b; modified with permission from Elsevier) for exhumation of ultrahigh-pressure (UHP) eclogite. (*e*) Model for expulsion of high-pressure eclogite along the trace of the Main Himalayan Thrust (Corrie et al. 2010; modified with permission from Elsevier), analogous to the numerical LHO-2 model of Beaumont et al. (2006). (*f*) Crustal aneurysm model for exhumation of syntaxis granulites (Zeitler et al. 2001a,b), illustrating how rapid erosion couples with weak partially molten rocks.

crust to thicker and stronger continental crust may introduce a relatively stiff plunger to the wedge and force rapid UHP exhumation (**Figure 12c**). Slab breakoff can also occur, especially for slow subduction, but models suggest that UHP rocks then ascend not as discrete thrust slices but as diapirs (**Figure 12d**). For fast subduction rates of approximately 5 cm/yr, each of these models predicts P-T paths involving nearly isothermal exhumation, commensurate with observed P-T paths (**Figure 6a**).

Formation of eclogites after initial collision is unsurprising because many thermal models predict eclogite-facies conditions along the MHT (e.g., Henry et al. 1997). Thus, tectonic interpretations of younger eclogites center on their exhumation and relation to the granulite-facies overprint. Two models have been proposed (Groppo et al. 2007, Corrie et al. 2010) that both appeal to singular events in the context of UHP and orogenic wedge models. Possibly, analogous to exhumation of UHP rocks, the eclogites were detached from subducting continental lithosphere, accreted to the base of the Himalayan wedge, and exhumed along the MHT (**Figure 12a,d**). Heating to reach granulite-facies conditions resulted from slow initial exhumation. Alternatively, inasmuch as Himalayan isotherms are inherently sigmoidal, upward expulsion of eclogites within the orogenic wedge (e.g., Beaumont et al. 2006) could lead to increasing T with decreasing P, causing a granulite-facies overprint (**Figure 12e**). The granulitized eclogites occur in the same belt as the high-T, low-P metamorphic overprint. Presumably, mechanisms of high-T overprinting—either polymetamorphism or rapid exhumation—could apply to the eclogites and their host gneisses.

Three models are proposed to explain the occurrence of syntaxial granulites. As with the eclogites, late-stage slab breakoff might catalyze exposure (Xu et al. 2010). Local cross-compression in the bend region could also lead to high-amplitude folding or a pop-up structure (Burg et al. 1998, Schneider et al. 1999). Alternatively, the tectonic aneurysm model (**Figure 4f**) links structural development and exposure to rapid erosion (Zeitler et al. 2001a,b; Koons et al. 2002). Rapid erosion bows isotherms, leading to partial melting, crustal weakening, and focused midcrustal flow, which maintains topography and balances rapid erosion. Like channel flow, as material is removed at the surface, midcrustal material flows laterally and upward to replace it. Although several rivers traverse the Himalayan range, the Indus and Yarlung Tsangpo have far greater discharge, promoting some of the highest erosion rates on Earth (Zeitler et al. 2001b). Predicted P-T trajectories (Koons et al. 2002) show exhumation from 775°C, 9 kbar to 675°C, 4 kbar, broadly compatible with P-T paths from the syntaxes (**Figure 7**).

SUMMARY POINTS

1. Despite some false starts, most petrologic investigations now recover P-T conditions and paths that are consistent with phase equilibria and petrologic models of mineral compositional zoning. These data quantify P-T gradients and paths across major thrust systems, although high Ts and complex reaction textures in the GHS have led to interpretational ambiguities. The steep P-T gradient across the MCT reflects protracted thrusting along a thin thrust zone, whereas the shallow gradient in the LHD reflects accumulation of small-displacement, in-sequence thrusts. Many named thrusts represent former traces of the MHT.

2. UHP eclogites formed ca. 45–55 Ma and initially exhumed isothermally or with cooling, but with thermal overprinting at moderate P. Such paths are consistent with several different modes of UHP exhumation, including corner flow, diapiric rise, and plunger

tectonics. Younger (ca. 25 Ma), lower-P, granulitized eclogites from eastern Nepal through western Bhutan show substantially more heating, possibly related to thermal overprinting in the region or expulsion upward in the context of overturned isotherms. A crustal aneurysm model is commonly invoked to explain exhumation of granulites in the syntaxes. Although this model is plausible, petrologic and chronologic data have yielded conflicting results.

3. Accessory mineral microanalysis is revolutionizing petrologic and tectonic investigations. Monazite-based T-t histories are consistent with in-sequence thrusting in Nepal. Titanite T-t histories as determined microanalytically constrain prograde heating rates. Leucogranite and Zrc Ts are difficult to reconcile with regional petrologic patterns, however.

4. Petrologic data from the LHS and THS generally rule out differential heat transport via flowing channels and thus favor critical wedge models. Petrologic and chronologic evidence in favor of channel flow is arguably limited to isothermal exhumation in the GHS in the eastern Nepal–western Bhutan sector. Evidence for orogenic flattening is found in several transects but is relatively understudied.

FUTURE ISSUES

1. The renaissance in accessory mineral petrogenesis, geochemistry, and microanalysis, especially the direct correlation between trace element thermometry and U-Pb geochronology in titanite and zircon, promises substantial rewards for constraining metamorphic and tectonic rates. Petrologists have long emphasized petrogenetic models to explain chemical variations in minerals. Geochronologists must do the same, i.e., characterize chemical domains and target chronologic analysis accordingly.

2. The ages and conditions of leucogranite emplacement have proven difficult to reconcile with independent P-T-t data, especially when high petrologic Ts are compared with low zircon and magmatic Ts. Excepting large leucogranite bodies, tectonically motivated chronologic research on leucogranites and migmatites cannot proceed without resolving these petrogenetic ambiguities.

3. Few studies quantify P-T conditions or P-T-t paths for rocks that span the STDS. Validating models of extension in compressional settings will require better characterization of THS metamorphism.

4. Refined chronologic analysis is warranted for UHP eclogites and syntaxial granulites using chemically and mineralogically fingerprinted mineral domains.

5. Further petrologic and chronologic investigation is needed for GHS rocks, wherein post-peak, high-T processes overprint and mask structures.

DISCLOSURE STATEMENT

ACKNOWLEDGMENTS

LITERATURE CITED

Beaumont C, Jamieson RA, Nguyen MH, Lee B. 2001. Himalayan tectonics explained by extrusion of a low-viscosity crustal channel coupled to focused surface denudation. *Nature* 414:738–42

Beaumont C, Nguyen MH, Jamieson RA, Ellis S. 2006. Crustal flow modes in large hot orogens. See Law et al. 2006, pp. 91–145

Berthelsen A. 1953. On the geology of the Rupshu District, NW Himalaya. *Medd. Dan. Geol. Foren.* 12:350–415

Beyssac O, Bollinger L, Avouac JP, Goffe B. 2004. Thermal metamorphism in the lesser Himalaya of Nepal determined from Raman spectroscopy of carbonaceous material. *Earth Planet. Sci. Lett.* 225:233–41

Boehnke P, Watson EB, Trail D, Harrison TM, Schmitt AK. 2013. Zircon saturation re-revisited. *Chem. Geol.* 251:324–34

Bookhagen B, Burbank DW. 2006. Topography, relief, and TRMM-derived rainfall variations along the Himalaya. *Geophys. Res. Lett.* 33:L08405

Booth AL, Chamberlain CP, Kidd WSF, Zeitler PK. 2009. Constraints on the metamorphic evolution of the eastern Himalayan syntaxis from geochronologic and petrologic studies of Namche Barwa. *Geol. Soc. Am. Bull.* 121:385–407

Booth AL, Zeitler PK, Kidd WSF, Wooden J, Liu Y, et al. 2004. U-Pb zircon constraints on the tectonic evolution of southeastern Tibet, Namche Barwa area. *Am. J. Sci.* 304:889–929

Burbank DW, Blythe AE, Putkonen J, Pratt-Sitaula B, Gabet E, et al. 2003. Decoupling of erosion and precipitation in the Himalayas. *Nature* 426:652–55

Burchfiel BC, Royden LH. 1985. North–south extension within the convergent Himalayan region. *Geology* 13:679–82

Burg J-P, Nievergelt P, Oberli F, Seward D, Davy P, et al. 1998. The Namche Barwa syntaxis: evidence for exhumation related to compressional crustal folding. *J. Asian Earth Sci.* 16:239–52

Butler RW, Harris NBW, Whittington AG. 1997. Interactions between deformation, magmatism and hydrothermal activity during active crustal thickening: a field example from Nanga Parbat, Pakistan Himalayas. *Mineral. Mag.* 61:37–52

Carosi R, Montomoli C, Rubatto D, Visona D. 2010. Late Oligocene high-temperature shear zones in the core of the Higher Himalayan Crystallines (Lower Dolpo, western Nepal). *Tectonics* 29:TC2400

Carosi R, Montomoli C, Rubatto D, Visona D. 2013. Leucogranite intruding the South Tibetan Detachment in western Nepal: implications for exhumation models in the Himalayas. *Terra Nova* 25:478–89

Catlos EJ, Harrison TM, Kohn MJ, Grove M, Ryerson FJ, et al. 2001. Geochronologic and thermobarometric constraints on the evolution of the Main Central Thrust, central Nepal Himalaya. *J. Geophys. Res.* 106(B8):16177–204

Cattin R, Avouac J-P. 2000. Modeling mountain building and the seismic cycle in the Himalaya of Nepal. *J. Geophys. Res.* 105(B6):13389–407

Chambers JA, Caddick M, Argles T, Horstwood M, Sherlock S, et al. 2009. Empirical constraints on extrusion mechanisms from the upper margin of an exhumed high-grade orogenic core, Sutlej valley, NW India. *Tectonophysics* 477:77–92

Chambers JA, Kohn MJ. 2012. Titanium in muscovite, biotite, and hornblende: modeling, thermometry and rutile activities in metapelites and amphibolites. *Am. Mineral.* 97:543–55

Chemenda AI, Burg J-P, Mattauer M. 2000. Evolutionary model of the Himalaya-Tibet system; geopoem based on new modelling, geological and geophysical data. *Earth Planet. Sci. Lett.* 174:397–409

Corrie SL, Kohn MJ. 2011. Metamorphic history of the central Himalaya, Annapurna region, Nepal, and implications for tectonic models. *Geol. Soc. Am. Bull.* 123:1863–79

Corrie SL, Kohn MJ, McQuarrie N, Long SP. 2012. Flattening the Bhutan Himalaya. *Earth Planet. Sci. Lett.* 349–350:67–74

Corrie SL, Kohn MJ, Vervoort JD. 2010. Young eclogite from the Greater Himalayan Sequence, Arun Valley, eastern Nepal: P-T-t path and tectonic implications. *Earth Planet. Sci. Lett.* 289:406–16

Cottle JM, Jessup MJ, Newell DL, Horstwood MSA, Noble SR, et al. 2009. Geochronology of granulitized eclogite from the Ama Drime Massif: implications for the tectonic evolution of the South Tibetan Himalaya. *Tectonics* 28:TC1002

Dahlen FA. 1990. Critical taper model of fold-and-thrust belts and accretionary wedges. *Annu. Rev. Earth Planet. Sci.* 18:55–99

Daniel CG, Hollister LS, Parrish RR, Grujic D. 2003. Exhumation of the Main Central Thrust from lower crustal depths, Eastern Bhutan Himalaya. *J. Metamorph. Geol.* 21:317–34

Dasgupta S, Ganguly J, Neogi S. 2004. Inverted metamorphic sequence in the Sikkim Himalayas: crystallization history, P-T gradient and implications. *J. Metamorph. Geol.* 22:395–412

Davidson C, Grujic DE, Hollister LS, Schmid SM. 1997. Metamorphic reactions related to decompression and synkinematic intrusion of leucogranite, High Himalayan Crystallines, Bhutan. *J. Metamorphic Geol.* 15:593–612

Day HW. 2012. A revised diamond-graphite transition curve. *Am. Mineral.* 97:52–62

de Sigoyer J, Chavagnac V, Blichert-Toft J, Villa IM, Luais B, et al. 2000. Dating the Indian continental subduction and collisional thickening in the northwest Himalaya: multichronology of the Tso Morari eclogites. *Geology* 28:487–90

de Sigoyer J, Guillot S, Dick P. 2004. Exhumation of the ultrahigh-pressure Tso Morari unit in eastern Ladakh (NW Himalaya): a case study. *Tectonics* 23:TC3003

de Sigoyer J, Guillot S, Lardeaux J-M, Mascle G. 1997. Glaucophane-bearing eclogites in the Tso Morari dome (eastern Ladakh, NW Himalaya). *Eur. J. Mineral.* 9:1073–83

DeCelles PG, Robinson DM, Quade J, Ojha TP, Garzione CN, et al. 2001. Stratigraphy, structure, and tectonic evolution of the Himalayan fold-thrust belt in western Nepal. *Tectonics* 20:487–509

Ding L, Zhong D. 1999. Metamorphic characteristics and geotectonic implications of the high-pressure granulites from Namjagbarwa, eastern Tibet. *Sci. China D* 42:491–505

Ding L, Zhong DL, Yin A, Kapp P, Harrison TM. 2001. Cenozoic structural and metamorphic evolution of the eastern Himalayan syntaxis (Namche Barwa). *Earth Planet. Sci. Lett.* 192:423–38

Donaldson DG, Webb AAG, Menold CA, Kylander-Clark ARC, Hacker BR. 2013. Petrochronology of Himalayan ultrahigh-pressure eclogite. *Geology* 41:835–38

England P, Molnar P. 1993a. Cause and effect among thrust and normal faulting, anatectic melting and exhumation in the Himalaya. See Treloar & Searle 1993, pp. 401–11

England P, Molnar P. 1993b. The interpretation of inverted metamorphic isograds using simple physical calculations. *Tectonics* 12:145–57

Evans J, Zalasiewicz J. 1996. U-Pb, Pb-Pb and Sm-Nd dating of authigenic monazite: implications for the diagenetic evolution of the Welsh Basin. *Earth Planet. Sci. Lett.* 144:421–33

Florence FP, Spear FS. 1991. Effects of diffusional modification of garnet growth zoning on P-T path calculations. *Contrib. Mineral. Petrol.* 107:487–500

Gaidies F, De Capitani C, Abart R. 2008. THERIA_G: a software program to numerically model prograde garnet growth. *Contrib. Mineral. Petrol.* 155:657–71

Ganguly J, Dasgupta S, Cheng W, Neogi S. 2000. Exhumation history of a section of the Sikkim Himalayas, India: records in the metamorphic mineral equilibria and compositional zoning of garnet. *Earth Planet. Sci. Lett.* 183:471–86

Godin L, Grujic D, Law RD, Searle MP. 2006. Channel flow, ductile extrusion and exhumation in continental collision zones: an introduction. See Law et al. 2006, pp. 1–23

Groppo C, Lombardo B, Rolfo F, Pertusati P. 2007. Clockwise exhumation path of granulitized eclogites from the Ama Drime range (Eastern Himalayas). *J. Metamorph. Geol.* 25:51–75

Groppo C, Rolfo F, Indares A. 2012. Partial melting in the Higher Himalayan Crystallines of eastern Nepal: the effect of decompression and implications for the "channel flow" model. *J. Petrol.* 53:1057–88

Groppo C, Rolfo F, Mosca P. 2013. The cordierite-bearing anatectic rocks of the higher Himalayan crystallines (eastern Nepal): low-pressure anatexis, melt productivity, melt loss and the preservation of cordierite. *J. Metamorph. Geol.* 31:187–204

Groppo C, Rubatto D, Rolfo F, Lombardo B. 2010. Early Oligocene partial melting in the Main Central Thrust Zone (Arun valley, eastern Nepal Himalaya). *Lithos* 118:287–301

Grujic D, Casey M, Davidson C, Hollister LS, Kundig R, et al. 1996. Ductile extrusion of the Higher Himalayan Crystalline in Bhutan: evidence from quartz microfabrics. *Tectonophysics* 260:21–43

Grujic D, Warren CJ, Wooden JL. 2011. Rapid synconvergent exhumation of Miocene-aged lower orogenic crust in the eastern Himalaya. *Lithosphere* 3:346–66

Guillot S, de Sigoyer J, Lardeaux JM, Mascle G. 1997. Eclogitic metasediments from the Tso Morari area (Ladakh, Himalaya): evidence for continental subduction during India-Asia convergence. *Contrib. Mineral. Petrol.* 128:197–212

Guillot S, Lardeaux JM, Mascle G, Colchen M. 1995. A new record of high-pressure metamorphism in the Himalayan Range—the retrogressed eclogites of the Tso Morari dome (east Ladakh). *C.R. Acad. Sci. II* 320:931–36

Guillot S, Mahéo G, de Sigoyer J, Hattori KH, Pêcher A. 2008. Tethyan and Indian subduction viewed from the Himalayan high- to ultrahigh-pressure metamorphic rocks. *Tectonophysics* 451:225–41

Guilmette C, Indares A, Hébert R. 2011. High-pressure anatectic paragneisses from the Namche Barwa, Eastern Himalayan Syntaxis: textural evidence for partial melting, phase equilibria modeling and tectonic implications. *Lithos* 124:66–81

Harris NBW, Caddick M, Kosler J, Goswami S, Vance D, Tindle AG. 2004. The pressure-temperature-time path of migmatites from the Sikkim Himalaya. *J. Metamorph. Geol.* 22:249–64

Harris NBW, Massey J. 1994. Decompression and anatexis of Himalayan metapelites. *Tectonics* 13:1537–46

Harrison TM, Célérier J, Aikman AB, Hermann J, Heizler MT. 2009. Diffusion of ^{40}Ar in muscovite. *Geochim. Cosmochim. Acta* 73:1039–51

Harrison TM, Grove M, McKeegan KD, Coath CD, Lovera OM, Le Fort P. 1999. Origin and episodic emplacement of the Manaslu intrusive complex, Central Himalaya. *J. Petrol.* 40:3–19

Harrison TM, Ryerson FJ, Le Fort P, Yin A, Lovera OM, Catlos EJ. 1997. A Late Miocene–Pliocene origin for the Central Himalayan inverted metamorphism. *Earth Planet. Sci. Lett.* 146:E1–7

Hayden LA, Watson EB, Wark DA. 2008. A thermobarometer for sphene (titanite). *Contrib. Mineral. Petrol.* 155:529–40

Hemingway BS, Bohlen SR, Hankins WB, Westrum EF Jr, Kuskov OL. 1998. Heat capacity and thermodynamic properties for coesite and jadeite, reexamination of the quartz-coesite equilibrium boundary. *Am. Mineral.* 83:409–18

Henry P, LePichon X, Goffe B. 1997. Kinematic, thermal and petrological model of the Himalayas: constraints related to metamorphism within the underthrust Indian crust and topographic elevation. *Tectonophysics* 273:31–56

Herman F, Copeland P, Avouac J-P, Bollinger L, Mahéo G, et al. 2010. Exhumation, crustal deformation, and thermal structure of the Nepal Himalaya derived from inversion of thermochronological and thermobarometric data and modeling of the topography. *J. Geophys. Res.* 115:B06407

Holland TJB. 1980. The reaction albite = jadeite + quartz determined experimentally in the range 600–1200°C. *Am. Mineral.* 65:129–34

Hubbard MS. 1996. Ductile shear as a cause of inverted metamorphism: example from the Nepal Himalaya. *J. Geol.* 104:493–99

Huerta AD, Royden LH, Hodges KV. 1999. The effects of accretion, erosion and radiogenic heat on the metamorphic evolution of collisional orogens. *J. Metamorph. Geol.* 17:349–66

Imayama T, Takeshita T, Arita K. 2010. Metamorphic P-T profile and P-T path discontinuity across the far-eastern Nepal Himalaya: investigation of channel flow models. *J. Metamorph. Geol.* 28:527–49

Inger S, Harris NBW. 1992. Tectonothermal evolution of the High Himalayan crystalline sequence, Langtang Valley, northern Nepal. *J. Metamorph. Geol.* 10:439–52

Jain AK, Manickavasagam RM. 1993. Inverted metamorphism in the intracontinental ductive shear zone during Himalayan collisional tectonics. *Geology* 21:407–10

Jamieson RA, Beaumont C, Medvedev S, Nguyen MH. 2004. Crustal channel flows: 2. Numerical models with implications for metamorphism in the Himalayan-Tibetan orogen. *J. Geophys. Res.* 109:B06407

Kaneko Y, Katayama I, Yamamoto H, Misawa K, Ishikawa M, et al. 2003. Timing of Himalayan ultrahigh-pressure metamorphism: sinking rate and subduction angle of the Indian continental crust beneath Asia. *J. Metamorph. Geol.* 21:589–99

Kellett DA, Grujic D, Coutand I, Cottle J, Mukul M. 2013. The South Tibetan detachment system facilitates ultra rapid cooling of granulite-facies rocks in Sikkim Himalaya. *Tectonics* 32:252–70

Kelsey DE, Clark C, Hand M. 2008. Thermobarometric modelling of zircon and monazite growth in melt-bearing systems: examples using model metapelitic and metapsammitic granulites. *J. Metamorph. Geol.* 26:199–212

Kelsey DE, Powell R. 2011. Progress in linking accessory mineral growth and breakdown to major mineral evolution in metamorphic rocks: a thermodynamic approach in the Na_2O-CaO-K_2O-FeO-MgO-Al_2O_3-SiO_2-H_2O-TiO_2-ZrO_2 system. *J. Metamorph. Geol.* 29:151–66

Kohn MJ. 2004. Oscillatory- and sector-zoned garnets record cyclic (?) rapid thrusting in central Nepal. *Geochem. Geophys. Geosyst.* 5:Q12014

Kohn MJ. 2007. *Paleoaltimetry—Geochemical and Thermodynamic Approaches*. Washington, DC: Mineral. Soc. Am.

Kohn MJ. 2008. P-T-t data from central Nepal support critical taper and repudiate large-scale channel flow of the Greater Himalayan Sequence. *Geol. Soc. Am. Bull.* 120:259–73

Kohn MJ. 2013. Geochemical zoning in metamorphic minerals. In *The Crust*, ed. RL Rudnick, pp. 229–61. Treatise Geochem. 3. Oxford, UK: Elsevier. 2nd ed.

Kohn MJ, Catlos EJ, Ryerson FJ, Harrison TM. 2001. Pressure-temperature-time path discontinuity in the Main Central thrust zone, central Nepal. *Geology* 29:571–74

Kohn MJ, Corrie SL. 2011. Preserved Zr-temperatures and U-Pb ages in high-grade metamorphic titanite: evidence for a static hot channel in the Himalayan orogen. *Earth Planet. Sci. Lett.* 311:136–43

Kohn MJ, Parkinson CD. 2002. Petrologic case for Eocene slab breakoff during the Indo-Asian collision. *Geology* 30:591–94

Kohn MJ, Spear F. 2000. Retrograde net transfer reaction insurance for pressure-temperature estimates. *Geology* 28:1127–30

Kohn MJ, Wieland MS, Parkinson CD, Upreti BN. 2004. Miocene faulting at plate tectonic velocity in the Himalaya of central Nepal. *Earth Planet. Sci. Lett.* 228:299–310

Kohn MJ, Wieland MS, Parkinson CD, Upreti BN. 2005. Five generations of monazite in Langtang gneisses: implications for chronology of the Himalayan metamorphic core. *J. Metamorph. Geol.* 23:399–406

Koons PO, Zeitler PK, Chamberlain CP, Craw D, Meltzer AS. 2002. Mechanical links between erosion and metamorphism in Nanga Parbat, Pakistan Himalaya. *Am. J. Sci.* 302:749–73

Lanari P, Riel N, Guillot S, Vidal O, Schwartz S, et al. 2013. Deciphering high-pressure metamorphism in collisional context using microprobe mapping methods: application to the Stak eclogitic massif (northwest Himalaya). *Geology* 41:111–14

Lavé J, Avouac JP. 2001. Fluvial incision and tectonic uplift across the Himalayas of central Nepal. *J. Geophys. Res.* 106(B11):26561–91

Law RD, Searle MP, Godin L, eds. 2006. *Channel Flow, Ductile Extrusion and Exhumation in Continental Collision Zones*. Geol. Soc. Spec. Publ. 268. London: Geol. Soc. Lond.

Le Fort P. 1975. Himalayas: the collided range. Present knowledge of the continental arc. *Am. J. Sci.* 275-A:1–44

Le Fort P, Guillot S, Pêcher A. 1997. HP metamorphic belt along the Indus suture zone of NW Himalaya: new discoveries and significance. *C.R. Acad. Sci. IIA* 325:773–78

Liu Y, Siebel W, Theye T, Massonne H-J. 2011. Isotopic and structural constraints on the late Miocene to Pliocene evolution of the Namche Barwa area, eastern Himalayan syntaxis, SE Tibet. *Gondwana Res.* 19:894–909

Liu Y, Zhong D. 1997. Petrology of high-pressure granulites from the eastern Himalayan syntaxis. *J. Metamorph. Geol.* 15:451–66

Lombardo B, Rolfo F. 2000. Two contrasting eclogite types in the Himalayas: implications for the Himalayan orogeny. *J. Geodyn.* 30:37–60

Lombardo B, Rolfo F, Compagnoni R. 2000. Glaucophane and barroisite eclogites from the Upper Kaghan Nappe: implications for the metamorphic history of the NW Himalaya. In *Tectonics of the Nanga Parbat Syntaxis and the Western Himalaya*, ed. MA Khan, PJ Treloar, MP Searle, MQ Jan, pp. 411–30. Geol. Soc. Spec. Publ. 170. London: Geol. Soc. Lond.

Long S, McQuarrie N. 2010. Placing limits on channel flow: insights from the Bhutan Himalaya. *Earth Planet. Sci. Lett.* 2010:375–90

Long S, McQuarrie N, Tobgay T, Grujic D. 2011. Geometry and crustal shortening of the Himalayan fold-thrust belt, eastern and central Bhutan. *Geol. Soc. Am. Bull.* 123:1427–47

Menard T, Spear FS. 1993. Metamorphism of calcic pelitic schists, Strafford Dome, Vermont; compositional zoning and reaction history. *J. Petrol.* 34:977–1005

Misch P. 1949. Metasomatic granitization of batholithic dimensions. *Am. J. Sci.* 247:209–45

Montomoli C, Iaccarino S, Carosi R, Langone A, Visona D. 2013. Tectonometamorphic discontinuities within the Greater Himalayan Sequence in Western Nepal (Central Himalaya): insights on the exhumation of crystalline rocks. *Tectonophysics* 608:1349–70

Mukherjee BK, Sachan HK. 2001. Discovery of coesite from Indian Himalaya: a record of ultra-high pressure metamorphism in Indian Continental Crust. *Curr. Sci.* 81:1358–61

Najman Y, Appel E, Boudagher-Fadel M, Bown P, Carter A, et al. 2010. Timing of India-Asia collision: geological, biostratigraphic, and palaeomagnetic constraints. *J. Geophys. Res.* 115:B12416

Neogi S, Dasgupta S, Fukuoka M. 1998. High P-T polymetamorphism, dehydration melting, and generation of migmatites and granites in the Higher Himalayan Crystalline Complex, Sikkim, India. *J. Petrol.* 39:61–99

O'Brien PJ, Zotov N, Law R, Khan MA, Jan MQ. 2001. Coesite in Himalayan eclogite and implications for models of India-Asia collision. *Geology* 29:435–38

Patiño Douce AE, Harris N. 1998. Experimental constraints on Himalayan anatexis. *J. Petrol.* 39:689–710

Pattison DRM. 1992. Stability of andalusite and sillimanite and the Al_2SiO_5 triple point; constraints from the Ballachulish aureole, Scotland. *J. Geol.* 100:423–46

Pattison DRM, Chacko T, Farquhar J, McFarlane CRM. 2003. Temperatures of granulite-facies metamorphism: constraints from experimental phase equilibria and thermobarometry corrected for retrograde exchange. *J. Petrol.* 44:867–900

Pearson ON, DeCelles PG. 2005. Structural geology and regional tectonic significance of the Ramgarh thrust, Himalayan fold-thrust belt of Nepal. *Tectonics* 24:TC4008

Pêcher A. 1989. The metamorphism in the central Himalaya. *J. Metamorphic Geol.* 7:31–41

Pinet C, Jaupart C. 1987. A thermal model for the distribution in space and time of the Himalayan granites. *Earth Planet. Sci. Lett.* 84:87–99

Pognante U, Benna P. 1993. Metamorphic zonation, migmatization and leucogranites along the Everest transect of eastern Nepal and Tibet; record of an exhumation history. See Treloar & Searle 1993, pp. 323–40

Pognante U, Piera B, Le Fort P. 1993. High-pressure metamorphism in the High Himalayan Crystallines of the Stak Valley, northeastern Nanga Parbat–Haramosh syntaxis, Pakistan Himalaya. See Treloar & Searle 1993, pp. 161–72

Pognante U, Spencer DA. 1991. First record of eclogites from the High Himalayan belt, Kaghan valley (northern Pakistan). *Eur. J. Mineral.* 3:613–18

Powell R, Holland T. 1994. Optimal geothermometry and geobarometry. *Am. Mineral.* 79:120–33

Pyle JM, Spear FS. 1999. Yttrium zoning in garnet: coupling of major and accessory phases during metamorphic reactions. *Geol. Mater. Res.* 1:1–49

Pyle JM, Spear FS. 2003. Four generations of accessory-phase growth in low-pressure migmatites from SW New Hampshire. *Am. Mineral.* 88:338–51

Rao RUM, Rao GV, Narain H. 1976. Radioactive heat generation and heat flow in the Indian shield. *Earth Planet. Sci. Lett.* 30:57–64

Rehman HU, Yamamoto H, Kaneko Y, Kausar AB, Murata M, Ozawa H. 2007. Thermobaric structure of the Himalayan Metamorphic Belt in Kaghan Valley, Pakistan. *J. Asian Earth Sci.* 29:390–406

Robinson DM, DeCelles PG, Garzione CN, Pearson ON, Harrison TM, Catlos EJ. 2003. Kinematic model for the Main Central thrust in Nepal. *Geology* 31:359–62

Robinson DM, Pearson ON. 2006. Exhumation of Greater Himalayan rock along the Main Central Thrust in Nepal: implications for channel flow. See Law et al. 2006, pp. 255–67

Royden LH. 1993. The steady state thermal structure of eroding orogenic belts and accretionary prisms. *J. Geophys. Res.* 98(B3):4487–507

Rubatto D. 2002. Zircon trace element geochemistry: partitioning with garnet and link between U-Pb ages and metamorphism. *Chem. Geol.* 184:123–38

Rubatto D, Chakraborty S, Dasgupta S. 2013. Timescales of crustal melting in the Higher Himalayan Crystallines (Sikkim, Eastern Himalaya) inferred from trace element–constrained monazite and zircon chronology. *Contrib. Mineral. Petrol.* 165:349–72

Sachan HK, Kohn MJ, Saxena A, Corrie SL. 2010. The Malari leucogranite, Garhwal Himalaya, northern India: chemistry, age, and tectonic implications. *Geol. Soc. Am. Bull.* 122:1865–76

Schlup M, Carter A, Cosca M, Steck A. 2003. Exhumation history of eastern Ladakh revealed by $^{40}Ar/^{39}Ar$ and fission-track ages: the Indus River–Tso Morari transect, NW Himalaya. *J. Geol. Soc.* 160:385–99

Schneider C, Masch L. 1993. The metamorphism of the Tibetan Series from the Manang area, Marsyandi Valley, Central Nepal. See Treloar & Searle 1993, pp. 357–74

Schneider DA, Edwards MA, Kidd WSF, Khan MA, Seeber L, Zeitler PK. 1999. Tectonics of Nanga Parbat, western Himalaya: synkinematic plutonism within the doubly vergent shear zones of a crustal-scale pop-up structure. *Geology* 27:999–1002

Searle MP. 1999. Emplacement of Himalayan leucogranites by magma injection along giant sill complexes: examples from the Cho Oyu, Gyachung Kang and Everest leucogranites (Nepal Himalaya). *J. Asian Earth Sci.* 17:773–83

Searle MP, Rex AJ. 1989. Thermal model for the Zanskar Himalaya. *J. Metamorph. Geol.* 7:127–34

Spear FS. 1993. *Metamorphic Phase Equilibria and Pressure-Temperature-Time Paths*. Washington, DC: Mineral. Soc. Am.

Spear FS, Cheney JT. 1989. A petrogenetic grid for pelitic schists in the system SiO_2-Al_2O_3-FeO-MgO-K_2O-H_2O. *Contrib. Mineral. Petrol.* 101:149–64

Spear FS, Kohn MJ, Cheney JT. 1999. P-T paths from anatectic pelites. *Contrib. Mineral. Petrol.* 134:17–32

Spear FS, Kohn MJ, Florence F, Menard T. 1990. A model for garnet and plagioclase growth in pelitic schists: implications for thermobarometry and P-T path determinations. *J. Metamorph. Geol.* 8:683–96

Spear FS, Peacock SM, Kohn MJ, Florence FP, Menard T. 1991. Computer programs for petrologic P-T-t path calculations. *Am. Mineral.* 76:2009–12

Spear FS, Pyle JM. 2010. Theoretical modeling of monazite growth in a low-Ca metapelite. *Chem. Geol.* 273:111–19

Spear FS, Selverstone J, Hickmott D, Crowley P, Hodges KV. 1984. P-T paths from garnet zoning: a new technique for deciphering tectonic processes in crystalline terranes. *Geology* 12:87–90

Stephenson BJ, Waters DJ, Searle MP. 2000. Inverted metamorphism and the Main Central thrust: field relations and thermobarometric constraints from the Kishtwar Window, NW Indian Himalaya. *J. Metamorph. Geol.* 18:571–90

St-Onge MR, Rayner N, Palin RM, Searle MP, Waters DJ. 2013. Integrated pressure-temperature-time constraints for the Tso Morari dome (Northwest India): implications for the burial and exhumation path of UHP units in the western Himalaya. *J. Metamorph. Geol.* 31:469–504

Su W, Zhang M, Liu XH, Lin JF, Ye K, Liu X. 2012. Exact timing of granulite metamorphism in the Namche Barwa, eastern Himalayan syntaxis: new constrains from SIMS U-Pb zircon age. *Int. J. Earth Sci.* 101:239–52

Swapp SM, Hollister LS. 1991. Inverted metamorphism within the Tibetan slab of Bhutan: evidence for a tectonically transported heat-source. *Can. Mineral.* 29:1019–41

Thiede RC, Ehlers TA, Bookhagen B, Strecker MR. 2009. Erosional variability along the northwest Himalaya. *J. Geophys. Res.* 114:F01015

Thomas JB, Watson EB, Spear FS, Shemella PT, Nayak SJ, Lanzirotti. 2010. TitaniQ under pressure: the effect of pressure and temperature on the solubility of Ti in quartz. *Contrib. Mineral. Petrol.* 160:743–59

Tonarini S, Villa IM, Oberli F, Meier M, Spencer DA, et al. 1993. Eocene age of eclogite metamorphism in Pakistan Himalaya; implications for India-Eurasia collision. *Terra Nova* 5:13–20

Tracy RJ, Robinson P, Thompson AB. 1976. Garnet composition and zoning in the determination of temperature and pressure of metamorphism, central Massachusetts. *Am. Mineral.* 61:762–75

Treloar PJ, O'Brien PJ, Parrish RR, Khan MA. 2003. Exhumation of early Tertiary, coesite-bearing eclogites from the Pakistan Himalaya. *J. Geol. Soc.* 160:367–76

Treloar PJ, Searle MP, eds. 1993. *Himalayan Tectonics*. Geol. Soc. Spec. Publ. 74. London: Geol. Soc. Lond.

Vance D, Mahar E. 1998. Pressure-temperature paths from P-T pseudosections and zoned garnets: potential, limitations and examples from the Zanskar Himalaya, NW India. *Contrib. Mineral. Petrol.* 132:225–45

Vannay JC, Grasemann B. 2001. Himalayan inverted metamorphism and syn-convergence extension as a consequence of a general shear extrusion. *Geol. Mag.* 138:253–76

Viskupic K, Hodges KV, Bowring SA. 2005. Timescales of melt generation and the thermal evolution of the Himalayan metamorphic core, Everest region, eastern Nepal. *Contrib. Mineral. Petrol.* 149:1–21

Visona D, Carosi R, Montomoli C, Tiepolo M, Peruzzo L. 2012. Miocene andalusite leucogranite in central-east Himalaya (Everest-Masang Kang area): low-pressure melting during heating. *Lithos* 144–45:194–208

Walker CB, Searle MP, Waters DJ. 2001. An integrated tectonothermal model for the evolution of the High Himalaya in western Zanskar with constraints from thermobarometry and metamorphic modeling. *Tectonics* 20:810–33

Warren CJ, Beaumont C, Jamieson RA. 2008a. Formation and exhumation of ultra-high-pressure rocks during continental collision: role of detachment in the subduction channel. *Geochem. Geophys. Geosyst.* 9:Q04019

Warren CJ, Beaumont C, Jamieson RA. 2008b. Modelling tectonic styles and ultra-high pressure (UHP) rock exhumation during the transition from oceanic subduction to continental collision. *Earth Planet. Sci. Lett.* 267:129–45

Waters DJ. 1991. Hercynite-quartz granulites: phase relations, and implications for crustal processes. *Eur. J. Mineral.* 3:367–86

Watson EB, Harrison TM. 1983. Zircon saturation revisited; temperature and composition effects in a variety of crustal magma types. *Earth Planet. Sci. Lett.* 64:295–304

Watson EB, Wark DA, Thomas JB. 2006. Crystallization thermometers for zircon and rutile. *Contrib. Mineral. Petrol.* 151:413–33

Webb AAG, Yin A, Harrison TM, Célérier J, Gehrels GE, et al. 2011. Cenozoic tectonic history of the Himachal Himalaya (northwestern India) and its constraints on the formation mechanism of the Himalayan orogen. *Geosphere* 7:1013–61

Whittington AG. 1996. Exhumation overrated at Nanga Parbat, northern Pakistan. *Tectonophysics* 260:215–26

Whittington AG, Harris N, Baker J. 2000. Low-pressure crustal anatexis: the significance of spinel and cordierite from metapelitic assemblages at Nanga Parbat, northern Pakistan. In *What Drives Metamorphism and Metamorphic Reactions?*, ed. PJ Treloar, PJ O'Brien, pp. 183–98. Geol. Soc. Spec. Publ. 138. London: Geol. Soc. Lond.

Wilke FDH, O'Brien PJ, Altenberger U, Konrad-Schmolke M, Khan MA. 2010a. Multi-stage reaction history in different eclogite types from the Pakistan Himalaya and implications for exhumation processes. *Lithos* 114:70–85

Wilke FDH, O'Brien PJ, Gerdes A, Timmerman MJ, Sudo M, Khan MA. 2010b. The multistage exhumation history of the Kaghan Valley UHP series, NW Himalaya, Pakistan from U-Pb and $^{40}Ar/^{39}Ar$ ages. *Eur. J. Mineral.* 22:703–19

Wilke FDH, Sobel ER, O'Brien PJ, Stockli DF. 2012. Apatite fission track and (U-Th)/He ages from the Higher Himalayan Crystallines, Kaghan Valley, Pakistan: implications for an Eocene Plateau and Oligocene to Pliocene exhumation. *J. Asian Earth Sci.* 59:14–23

Willett SD. 1999. Orogeny and orography: the effects of erosion on the structure of mountain belts. *J. Geophys. Res.* 104(B12):28957–81

Winslow DM, Chamberlain CP, Zeitler PK. 1995. Metamorphism and melting of the lithosphere due to rapid denudation, Nanga Parbat massif Himalaya. *J. Geol.* 103:395–409

Wyss M. 2000. Metamorphic evolution of the northern Himachal Himalaya: phase equilibria constraints and thermobarometry. *Schweiz. Mineral. Petrogr. Mitteil.* 80:317–50

Xu W-C, Zhang H-F, Parrish R, Harris N, Guo L, Yuan H-L. 2010. Timing of granulite-facies metamorphism in the eastern Himalayan syntaxis and its tectonic implications. *Tectonophysics* 485:231–44

Xu Z, Ji S, Cai Z, Zeng L, Geng Q, Cao H. 2012. Kinematics and dynamics of the Namche Barwa Syntaxis, eastern Himalaya: constraints from deformation, fabrics and geochronology. *Gondwana Res.* 21:19–36

Yin A. 2006. Cenozoic tectonic evolution of the Himalayan orogen as constrained by along-strike variation of structural geometry, exhumation history, and foreland sedimentation. *Earth-Sci. Rev.* 76:1–131

Yin A, Harrison TM. 2000. Geologic evolution of the Himalayan-Tibetan orogen. *Annu. Rev. Earth Planet. Sci.* 28:211–80

Zeitler PK, Chamberlain CP. 1991. Petrogenetic and tectonic significance of young leucogranites from the northwestern Himalaya, Pakistan. *Tectonics* 10:729–41

Zeitler PK, Chamberlain CP, Smith HA. 1993. Synchronous anatexis, metamorphism, and rapid denudation at Nanga Parbat (Pakistan Himalaya). *Geology* 21:347–50

Zeitler PK, Koons PO, Bishop MP, Chamberlain CP, Craw D, et al. 2001a. Crustal reworking at Nanga Parbat, Pakistan: metamorphic consequences of thermal-mechanical coupling facilitated by erosion. *Tectonics* 20:712–28

Zeitler PK, Meltzer AS, Koons PO, Craw D, Hallet B, et al. 2001b. Erosion, Himalayan geodynamics, and the geomorphology of metamorphism. *GSA Today* 11:4–9

Zhu XK, O'Nions RK. 1999. Zonation of monazite in metamorphic rocks and its implications for high temperature thermochronology; a case study from the Lewisian terrain. *Earth Planet. Sci. Lett.* 171:209–20